SEDIMENTOLOGY the journal of the International Association of Sedimentologists IAS

Sedimentology (2025) doi: 10.1111/sed.70063

Ichnological insights into deoxygenation across the Cenomanian–Turonian Boundary Oceanic Anoxic Event 2 in the northern extent of Western Interior Seaway (west-central Alberta)

SARA K. BIDDLE and MURRAY K. GINGRAS
Department of Earth and Atmospheric Sciences, University of Alberta, Edmonton, Alberta T6G 2E3, Canada (E-mail: biddle@ualberta.ca)

Associate Editor – John Reijmer

ABSTRACT

In-depth ichnological and sedimentological analyses of the Cenomanian–Turonian boundary Oceanic Anoxic Event (OAE2) from the Western Interior Seaway of west-central Alberta reveal a persistent physico-chemically stressed setting. The interval is characterised by a dominantly diminutive and diminished ichnological assemblage, with familiar ichnotaxa (e.g. *Phycosiphon*, *Chondrites*, *Nereites*, *Planolites*, *Teichichnus*, *Cylindrichnus* and *Palaeophycus*), fugichnia and navichnia ethological groups, and evidence of meiofaunal reworking and two other indistinct biodeformational fabrics. Grouping trace fossils into four ichnoguilds (the fugichnia ichnoguild, the *Planolites* ichnoguild, the *Phycosiphon* ichnoguild and the *Chondrites* ichnoguild) reveals fluctuating oxygen, salinity and sedimentation stress over time. Integrated analysis of ichnological characteristics, ichnofacies and ichnoguilds reveals five different bottom water oxygen scenarios, including: (i) poorly oxygenated, (ii) severely dysoxic, (iii) extremely dysoxic, (iv) episodic storm-injected oxygen and (v) anoxia. Comparing trace fossil data with carbon isotope data, where the OAE2 is defined as a positive excursion, reveals oxygen trends over the event. Oxygenation was found to be highest below the OAE2 and declined rapidly over the Cenomanian–Turonian boundary. The Cenomanian–Turonian boundary itself is characterised by low and constantly fluctuating depositional dissolved oxygen, but never persistent anoxia. Counterintuitively, the most deoxygenated interval occurs after the termination of the OAE2 event. The delayed onset of lowest oxygen levels may be due to peak transgression occurring post-OAE2 and slowed northward migration of warm oxygen-poor Tethyan waters.

Keywords anoxia, Cenomanian–Turonian Boundary, ichnology, Oceanic Anoxic Event 2, organic-rich mudstones, palaeo-oxygenation, Western Interior Seaway.

INTRODUCTION

Cretaceous oceanic anoxic events (OAEs) are widely recognised Mesozoic perturbations in the global carbon cycle. Individual events are defined by globally recognised positive carbon isotope excursions (CIE, $\delta^{13}C$), and often correspond to micro- and macrofossil extinctions and deposition of organic-rich horizons, both linked to poorly oxygenated bottom waters (Schlanger & Jenkyns, 1976; Jenkyns, 1980; Schlanger *et al.*, 1987; Leckie *et al.*, 2002). Perhaps the most well-known of these events is the short-lived OAE2 (~560 to 885 kyr; Sageman *et al.*, 2006), a global productivity event, that resulted in ostensibly globally distributed organic-rich mudstone layers (e.g. Arthur *et al.*, 1987; Takashima *et al.*, 2006; Trabucho Alexandre *et al.*, 2010) bracketing the Cretaceous Cenomanian–Turonian boundary (CTB, ~93.95 Ma; Singer *et al.*, 2025). Large igneous provinces (LIPs) have been recognised as the likely OAE2 forcing (Turgeon & Creaser, 2008). A LIP-associated rise in atmospheric CO_2 led to intense global warming and resulted in widespread ocean acidification and stratification (e.g. Barclay *et al.*, 2010; Jenkyns, 2018). The exact large igneous province responsible for the OAE2 event remains debated, but it likely resulted from multiple significant eruptive episodes, including those associated with the Caribbean Plateau (CLIP; Turgeon & Creaser, 2008), the Kerguelen Plateau (KLIP; Walker-Trivett *et al.*, 2024) and/or the High Arctic Large Igneous Province (HALIP; Dummann *et al.*, 2024). Extreme warming and deoxygenation were briefly punctuated early on by a presumed global cooling event (i.e. the Plenus Cold Event) and synchronous temporary re-oxygenation of oceanic waters (Jenkyns, 2018).

European and US localities containing the OAE2 have been extensively studied to reconstruct local, regional and global environmental and climate conditions during the Cenomanian–Turonian hot house. However, OAEs are poorly characterised in the Canadian portion of the North American Western Interior Seaway (WIS), and detailed ichnofossil analyses have yet to be completed for the majority of the North American mudstone sections. Furthermore, the full extent of deoxygenation in the WIS—including its lateral spread, duration and intensity—is not yet fully understood (e.g. the southern extent of the WIS within the United States is interpreted to reflect improved oxygenation within the lower half of the OAE2-bearing interval, and lacks evidence for expression of the Plenus Cold Event (Arthur & Sageman, 2005; Elderbak & Leckie, 2016; Lowery *et al.*, 2018; Sageman *et al.*, 2024)).

Trace fossils provide valuable insight into the dissolved oxygen concentration (DO_2) of bottom waters and surrounding pore waters that are not discernible from primary sedimentary structures or geochemical data alone (Bromley & Ekdale, 1984; Bromley, 1996; MacEachern *et al.*, 2007; Gingras *et al.*, 2011). Further, biogenic reworking directly reflects seawater and pore-water chemistry at the time of an organism's activities, whereas post-depositional processes such as advection of elements through pore water (Scott & Lyons, 2012), and bioturbation itself (Löwemark & Singh, 2024; Monedero-Contreras *et al.*, 2024), can alter geochemical data. In marine settings, even sediments that are partially oxygenated support some infauna and surface grazers. Within reason, trace fossil distributions and bioturbation extent before, during and after the OAE2 can be used to coarsely reconstruct DO_2 concentrations.

As warmer oceans hold less oxygen, studying ancient climactically induced low-oxygen environments like the WIS CTB interval can help predict and potentially mitigate future ocean response to ongoing climate change. Understanding depositional oxygenation also has economic utility. Conventionally, poorly oxygenated sediments are thought to have higher rates of preserved organic carbon, and thus more resource potential. Several formations deposited in the WIS during the Cenomanian–Turonian transition are indeed important source rocks and source-rock reservoirs (e.g. the Second White Specks Formation, the Eagle Ford Formation). Hence, understanding redox histories within a basin may help pinpoint hydrocarbon sweet spots (e.g. Demaison & Moore, 1980; Pratt, 1984; Tyson, 1987; Savrda & Bottjer, 1991).

This study uses trace fossils to interpret the extent of deoxygenation across the OAE2-bearing interval in a Western Canadian core. Integrating an extensive ichnological data set with sedimentology, total organic carbon measurements and carbon isotopes facilitated detailed interpretations of: (i) the total of the physicochemical stressors acting at the site of deposition; (ii) the relative extent of deoxygenation over the OAE2-bearing interval; and (iii) how this interval differs from other OAE2-bearing intervals in the WIS and globally.

GEOLOGICAL BACKGROUND

The Cretaceous interval in central Alberta is recorded by strata deposited within the Western Canadian Foreland Basin (WCFB), representing the northern part of the broader North American WIS (Fig. 1). Basin development began in the late Jurassic, initiated by the collision of terranes along the western edge of the North American Craton (Monger *et al.*, 1982), resulting in the Cordillera fold and thrust belt, subsequent foreland subsidence and the development of an east–west deepening asymmetrical epicontinental foreland basin (Price, 1973; Beaumont, 1981; Pană & van der Pluijm, 2015; Quinn *et al.*, 2016).

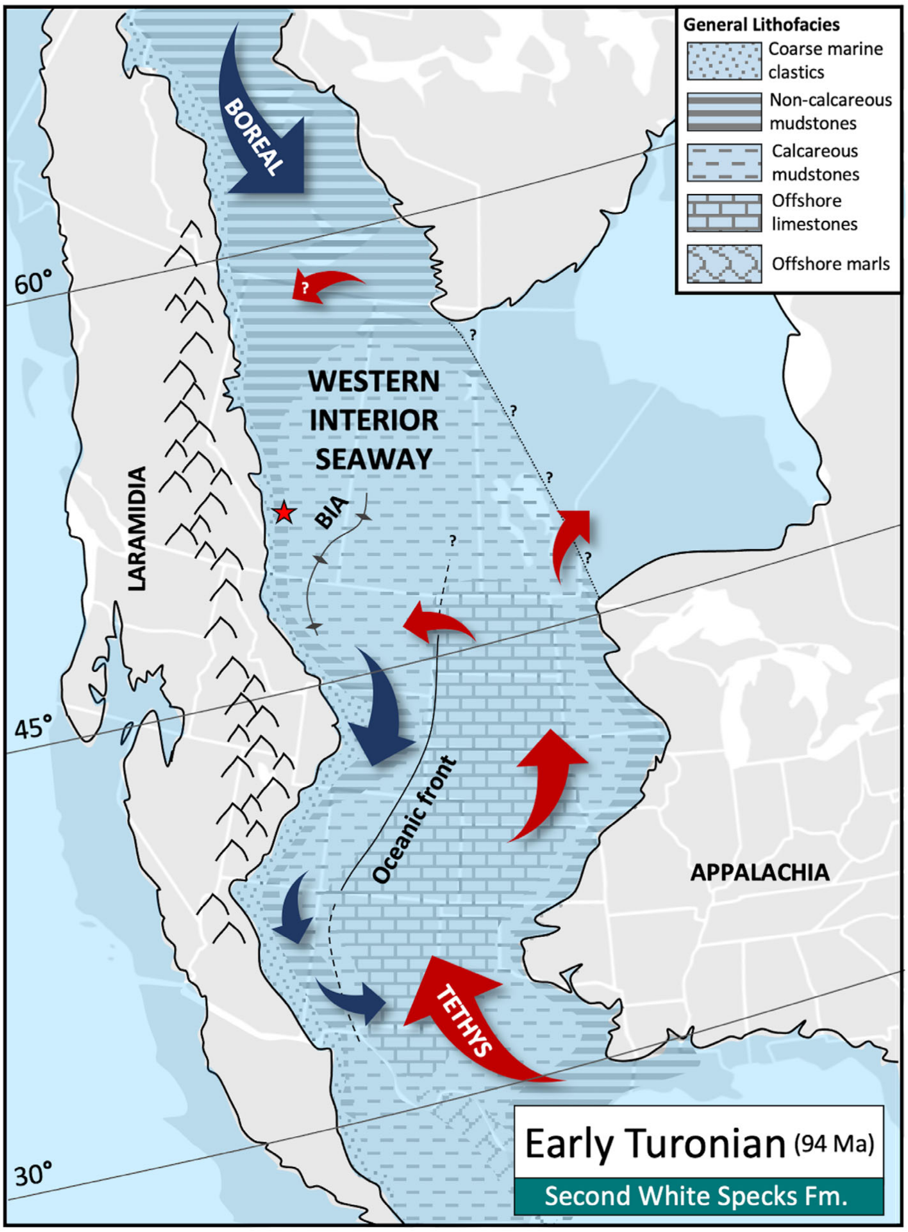

Fig. 1. Palaeogeography and general lithofacies of the Western Interior Seaway during the OAE2 (modified from Sageman & Arthur, 1994 and Blakey, 2014). Red star indicates core location, red arrows indicate warm normal salinity Tethyan-influenced waters and blue arrows indicate cold low-salinity Boreal-influenced waters. Location of palaeoceanographic fronts from Arthur & Sageman (2005) and Laurin & Sageman (2007). Approximate locations of frontal cross over (water mass circulation) modified from Slingerland *et al.* (1996) (northern USA) and Sageman *et al.* (2024) (northern Alberta). Location of the Bow Island Arch (BIA) after Wright (1994), representing a sub-aqueous palaeo-topographic high during the late Cenomanian through Early Turonian.

Palaeontologic and sedimentologic evidence indicate the Late Cenomanian WIS saw the influx of Tethyan waters infiltrating from the incipient Gulf of Mexico during the Greenhorn Transgression, resulting in significant expansion and widening of the seaway (Kauffman, 1977, 1984; Hancock & Kauffman, 1979; Kauffman & Caldwell, 1993). Warm southern-sourced normal-marine Tethyan waters commingled with the cold and low-salinity Boreal Sea waters intruding southwards from the proto-Arctic Ocean (Kauffman & Caldwell, 1993). A likely east–west-oriented oceanic front developed in the southern (American) part of the seaway (Fig. 1) as the Tethyan waters migrated north along the eastern edge (Leckie *et al.*, 1998; Fisher, 2003; Polyak, 2003; Arthur & Sageman, 2005; Laurin & Sageman, 2007; Corbett & Watkins, 2013; Elderbak *et al.*, 2014; Elderbak & Leckie, 2016; Lockshin *et al.*, 2017; Lowery *et al.*, 2018; Fortiz *et al.*, 2024), and counter-clockwise circulation was at least intermittent (potential circulation latitudes indicated by red arrows in Fig. 1) (Slingerland *et al.*, 1996; Arthur & Sageman, 2005; Elderbak & Leckie, 2016; Sageman *et al.*, 2024). Palaeontologic data and circulation models indicate potential Tethyan influence over the eastern edge of the Canadian portion of the WIS during the Cenomanian–Turonian transition (Schröder-Adams *et al.*, 1996; Hosseininejad Mohebati, 2016; Sageman *et al.*, 2024), but the extent of influence over present-day western Alberta and the location of a palaeo-oceanic front is so far undocumented.

The late Cenomanian through Early Turonian was a period of intense LIP-associated volcanism and outgassing of CO_2, which led to a warming climate (Vermeij, 1995; Leckie *et al.*, 2002; Turgeon & Creaser, 2008) and enhanced hydrologic cycle (i.e. continental weathering), increasing terrigenous nutrient influx into the seaway (e.g. Larson & Erba, 1999; Bryant *et al.*, 2021). These conditions, combined with the warm southern-sourced waters, triggered intense photic zone primary productivity. As a result, many areas within the WIS saw increased settling and preservation of organic carbon and carbonate (e.g. calcareous skeletons), with associated deposits recording the $+\delta^{13}C$ excursion that corresponds with the onset of the globally traceable OAE2 (positive $\delta^{13}C$ excursions indicate increased concentrations of the heavier ^{13}C isotope in organic matter and carbonates, reflecting ^{12}C depletion—a situation common in times of global increased organic matter burial) (Schlanger & Jenkyns, 1976; Arthur & Schlanger, 1979; Leckie *et al.*, 2002; Jenkyns, 2010). This intense productivity likely played a role in the development of poorly oxygenated bottom waters in the northern (Alberta) portion of the WIS (e.g. Percy & Pedersen, 2020). In contrast, the southern (US) portion of the WIS saw an increase in bottom water oxygenation during this time (e.g. poorly oxygenated Hartland Shale/Lower Eagle Ford Formation and the better oxygenated overlying Bridge Creek Limestone/Upper Eagle Ford Formation, Fig. 2), owing to improved circulation as Tethyan waters overtopped a southern Texan relict reef margin sill (Arthur & Sageman, 2005; French *et al.*, 2024). The initial oxygenation event to the south is concomitant with the 'Benthonic Zone', recording an abrupt increase in benthic foraminiferal assemblages (Eicher & Worstell, 1970), generally corresponding with the initial OAE2 + $\delta^{13}C$ excursion and the onset of the Plenus Cold Event identified in Europe.

The Late Cenomanian interval in west-central Alberta (red star in Fig. 1) is characterised by the deposition of the silty and slightly calcareous mudstones of the Belle Fourche Formation (Fig. 2). Continued deepening of the seaway and supposed higher productivity and associated organic influx to the sea floor led to the deposition of the more calcareous organic-rich mudstones of the Second White Specks Formation (2WS) in the late Cenomanian to early Turonian (Fig. 2). Third-order sea-level fluctuations continued throughout the deposition of the 2WS (Fig. 2; Haq, 2014) leading to internal stratal surfaces within the formation itself (e.g. 'Lower', 'Middle' and 'Upper' units separated by transgressive and regressive surfaces; Percy, 2021). A north-east plunging subaqueous topographic high running from northern Montana (the Sweetgrass Arch, SA) through southern Alberta and Saskatchewan (the Bow Island Arch, BIA) was located south-east of the cored location (Fig. 1) (Wells, 1957; Ridgley *et al.*, 1999). The BIA influenced depositional geometry in southern Alberta during the latest Cenomanian to early Turonian, forming axis-perpendicular transgressive sand ridges (Belle Fourche Formation) and carbonate ridges (Lower 2WS) (Percy, 2021). However, differential subsidence limited the BIA's impact during the deposition of the upper portion of the 2WS (Percy, 2021). Other detailed local palaeodepositional reconstructions for the western-edge 2WS interval are limited (e.g. Tyagi *et al.*, 2007; Plint *et al.*, 2012; Prokoph *et al.*, 2013; Lowery *et al.*, 2014; Percy & Pedersen, 2020; Percy, 2021), as the majority of studies conducted on the Western Canadian Cenomanian–Turonian interval are focused on the reservoir potential of the organic-rich 2WS (e.g. Stasiuk & Goodarzi, 1988; Furmann *et al.*, 2014, 2015, 2016; Boucher, 2016; Synnott *et al.*, 2017; Goodarzi *et al.*, 2022).

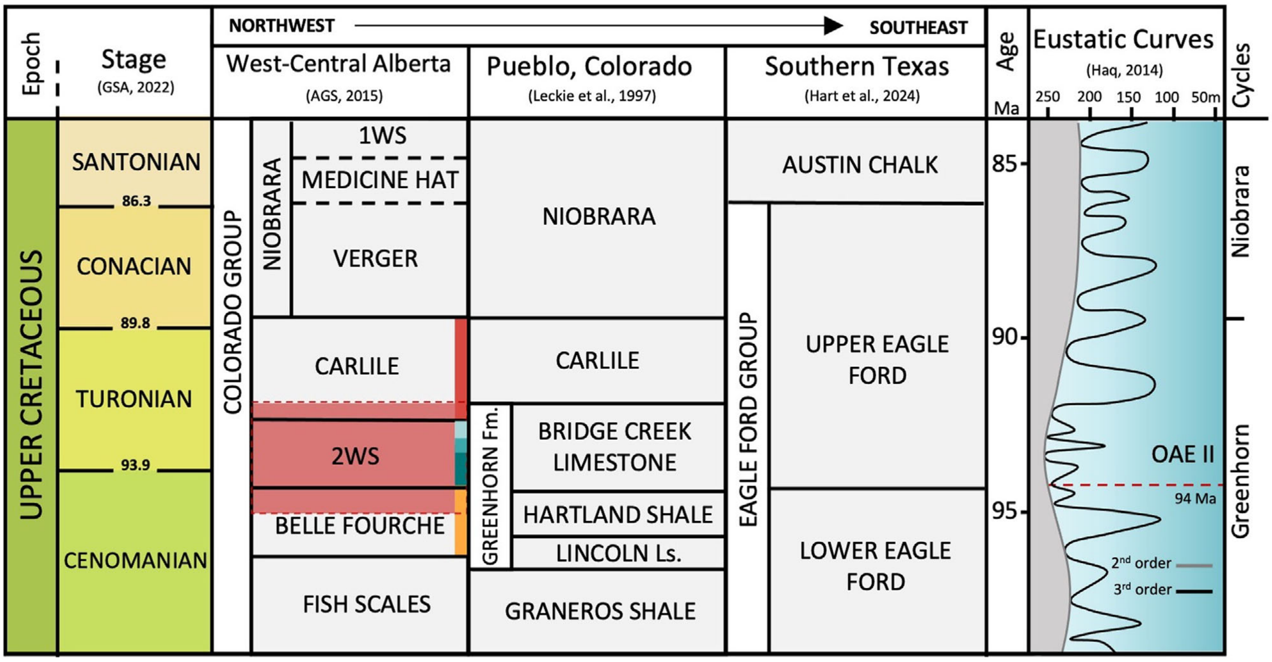

Fig. 2. Stratigraphic column modified from Percy & Pedersen (2020), Alberta Geological Survey (2015), Leckie *et al.* (1998) and Hart *et al.* (2024). Stage boundary dates from the Geological Society of America (updated 2022), eustatic seal level curves adapted from Haq (2014), OAE2 dates from Jones *et al.* (2021) and Dummann *et al.* (2024). The red shaded area indicates the studied core interval, and the colour stack to the right indicates internal stratigraphic boundaries referred to throughout this study (orange = Belle Fourche Formation, dark blue = Lower Second White Specks, medium blue = Middle Second White Specks, light blue = Upper Second White Specks and pink = Carlile Formation).

Prior research efforts describe the 2WS as deposited in a shallow (<70 m), sediment-starved setting with frequent seafloor reworking (Plint *et al.*, 2012; Percy & Pedersen, 2020). Previous analysis of the studied drill core suggests deposition occurred mainly through the transport of clay-mineral dominated silt- to sand-sized composite particles, including faecal pellets and intraclasts (Percy & Pedersen, 2020). The abundance of mud-dominated intraclasts confirms repeated cycles of deposition, erosion and redeposition, likely due to storm-wave reworking (Plint, 2014; Percy & Pedersen, 2020).

Conventionally, the lack of pervasive biogenic reworking throughout the 2WS, this core included, has been ascribed to fluctuating but low bottom water DO_2 concentrations (e.g. Schröder-Adams *et al.*, 1996; Synnott *et al.*, 2017; Percy & Pedersen, 2020). Beyond these simple interpretations, there has been no attempt to ichnologically analyse the extent of deoxygenation over the encapsulated OAE2 interval in Canada.

MATERIALS AND METHODS

This study examined a well-preserved, slabbed and nearly continuous >100-m-long drill core spanning the Upper Belle Fourche Formation and the entirety of the overlying 2WS Formation, located just northwest of Calgary, AB (Figs 1 to 3) (core details: Shale Petroleum's Boggy Lake 02/13-06-30-05W5/0 well, drilled summer 2014; associated horizontal well: Hz Boggy Lake 10-12-30-06W5, 98% recovery; the included basal portion of the Middle Turonian Carlile Formation was not evaluated herein). The core was evaluated for fine detail (<1 cm) sedimentological and ichnological characteristics before, during and after the OAE2.

Recognising discrete trace fossils, especially in the mud-dominated 2WS, is made difficult by the lack of significant lithologic contrast. Here, substantial care was taken to evaluate ichnological features at a millimetre scale. Detailed analysis involved examining washed core faces under various lighting conditions (e.g. regular overhead light, close-up high-intensity flashlight),

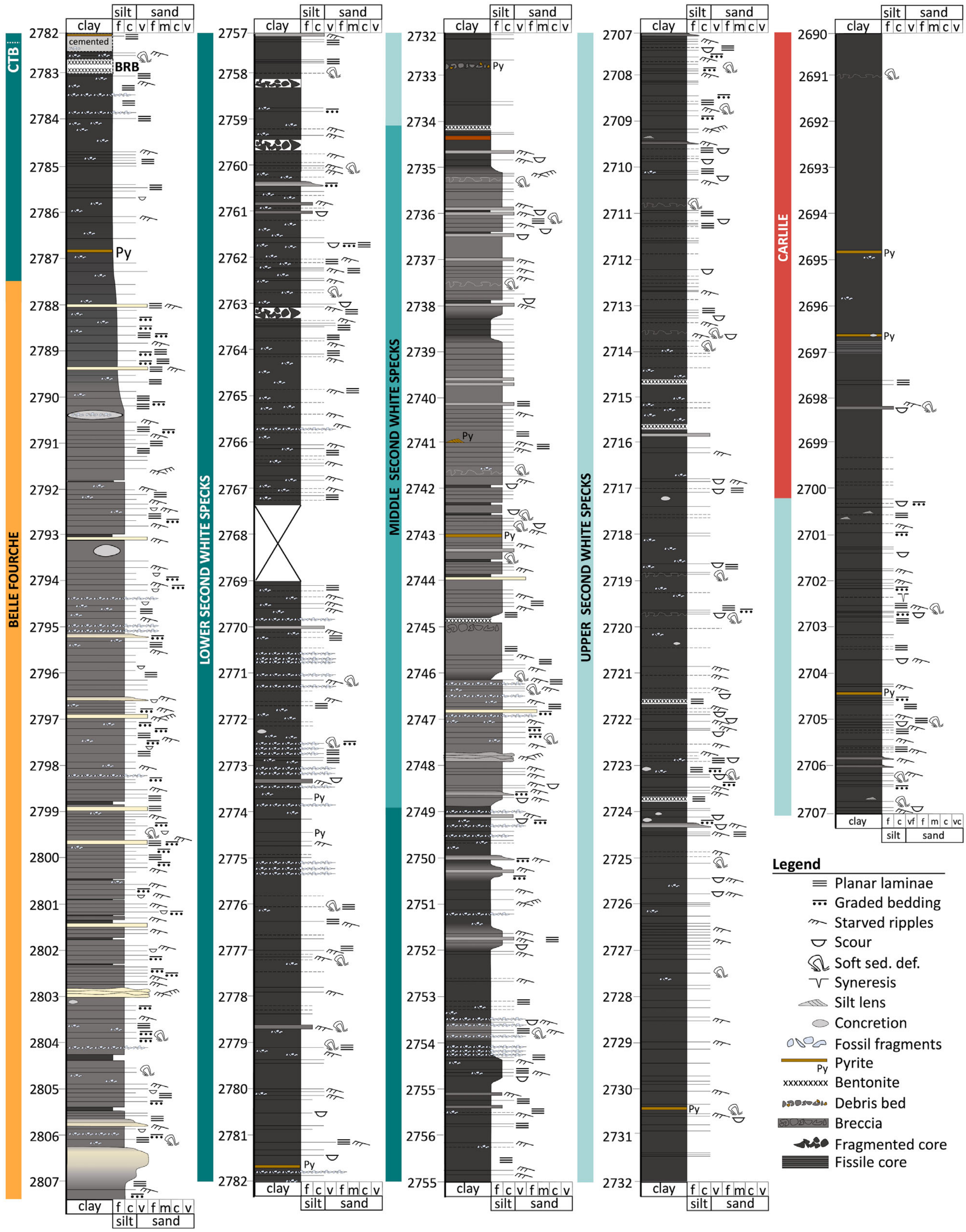

Fig. 3. Litholog of studied drill core.

with wet core providing the best contrast for identifying biogenic reworking. Unfortunately, the wet core photographed poorly, thus only dry photographs are included. Each naturally fractured bedding plane was inspected for horizontal trace fossils. Millimetre-scale sedimentological and ichnological observations were recorded in 10 cm intervals, including primary sedimentological structures, mineralogy, burrow size, diversity and Bioturbation Index (0 to 6; e.g. Taylor & Goldring, 1993). Further ichnological assessments included evaluating: (i) trace fossil types (i.e. the ethological characteristics of individual ichnotaxa), (ii) distributions of ichnogenera (e.g. changes in trace fossil diversity and ichnoguild distributions through time) and (iii) burrow size fluctuations (e.g. Gingras *et al.*, 2011).

Forty-four thin sections, originally sampled by Percy & Pedersen (2020) (currently held at the Core Research Center in Calgary as part of a public collection), were examined for further insight into sedimentological and ichnological characteristics. Following standard practice for organic-rich mudstone studies, thin sections were prepared 'ultra-thin' (<20 μm) to enhance the visibility of silt and mud-sized features and reduce opacity (Schieber, 1998; Macquaker & Adams, 2003; Lazar *et al.*, 2015a). The ultra-thin nature of the thin sections enhances birefringence; thus, staining thin sections for mineralogy is of heightened importance. All thin sections were stained with Alizarin Red-S for calcite (stains red), potassium ferricyanide for ferroan calcite (dark purple) and dolomite (blue) differentiation, and sodium cobaltinitrite for feldspar differentiation (k-spar stains yellow) (Percy & Pedersen, 2020).

Total organic carbon content and carbon isotope ratios ($\delta^{13}C_{org}$) were measured at 50 cm intervals. Core samples were first cleaned and rinsed with distilled water to remove any drilling mud or markings. A homogenised bulk 200 mesh powder was produced using an automated agate mortar and pestle. Splits from the homogenised powder were used for subsequent analyses. Programmed pyrolysis by HAWKTM was used to determine TOC content with ±5% analytical error based on analyses of a standard reference material (internal 9107 shale standard) every 5th sample. Carbon isotope samples were initially decarbonated by acid washing and then rinsed with distilled water until neutral. Carbon isotope ratios were then determined by Continuous Flow-Elemental Analysis-Isotope Ratio Mass Spectrometry (CF-EA-IRMS). Reported results are relative to the Vienna PeeDee Belemnite standard (V-PDB), with ±0.2 ‰ analytical error (based on internal lab standards calibrated against international standards, run every 5th sample). The TOC and carbon isotope values herein are likely true for their sampled depths, as burrow penetration depths over the entire cored interval are shallow (<1 cm) and would not have redistributed geochemical signatures more than several centimetres at most, certainly not beyond the 50 cm sample resolution.

In west-central Alberta, the transition between the siliceous mudstones of the Belle Fourche Formation and the more calcareous mudstones of 2WS is gradual (Tyagi *et al.*, 2007; Percy & Pedersen, 2020). The 'Bighorn River Bentonite' (BRB) is commonly picked as the formation contact on well logs (represented by a positive spike in gamma-ray and a negative spike in resistivity) (Bloch *et al.*, 1993; Tyagi *et al.*, 2007; Percy, 2021). In the studied core, the Belle Fourche–2WS formation boundary is placed at 2787.5 m depth, where a stark change from interbedded siltstone and mudstone to dark grey mudstone with common bivalve fragments occurs (after Percy & Pedersen, 2020). A hiatus at the CTB, within the upper portion of the OAE2 CIE, was identified in the Kaskapau Formation in northern Alberta (van Helmond *et al.*, 2016). This hiatus may be reflected herein as a ~ 25 cm thick well-cemented interval (~2782.15 m) roughly 20 cm above the Bighorn River Bentonite (Fig. 3). Without detailed palaeontologic data or age dating, the CTB herein has been placed at this cemented zone (2782.15 m), roughly coinciding with the recovery phase of the OAE2 as indicated by decreasing $\delta^{13}C$ values (carbon isotope data for this core clearly shows the positive excursion, concomitant with the OAE2, spanning 2781 to 2787.5 m). This is further consistent with the idea that the Bighorn River Bentonite is equivalent to the 'B Bentonite' in the southern (US) WIS, dated older than the CTB (Tyagi *et al.*, 2007; Barker *et al.*, 2011). Following the work of Percy & Pedersen (2020), the 2WS is divided into Lower (organic-rich calcareous mudstone, L2WS), Middle (quartz-rich silty mudstone, M2WS) and Upper (non-calcareous mudstone, U2WS) intervals based on mineralogy and grain size (and separated by transgressive and regressive surfaces).

Table 1. Facies descriptions and interpretations, and corresponding spilt core diagram (left). Shaded colours of each facies match the lithofacies colours on Figs 10 and 16.

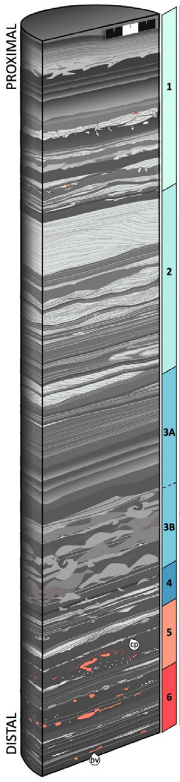

Facies	Facies Name	Sedimentology	Ichnology			Interpretation	Fig.
		Description	BI	Description	Ichnogenera		
1	**Interbedded normally graded and silt-rippled medium grey silty mudstone**	Ubiquitous normally graded beds and bed sets, with intercalated erosively-based wave ripples and low angle laminated siltstones. Soft sediment deformation is common. Carbonaceous detritus and wood fragments are sporadic to common along bedding planes, while syneresis cracks, calcareous pellets and bivalve fragments are rare.	0-6	Low diversity and diminutive suite Biogenic reworking fluctuates bed-by-bed Common top down (lam-scram) reworking	*Planolites, Phycosiphon, Teichichnus, Chondrites,* fugichnia, navichnia	Delta-derived hyperpycnal flows (e.g., hyperpycnites; potentially wave-propagated) with punctuating storms (tempestite beds) **River-dominated storm-influenced prodelta**	Fig. 4
2	**Poorly to moderately bioturbated interbedded rippled silt and medium grey mudstone**	Siltstone beds present as starved current ripples, combined flow ripples, wave ripples, and low angle laminated beds. Siltstone beds are often capped by structureless appearing mud. Normally graded beds are rare throughout. Soft sediment deformation occurs both as convolute bedding and flame structures. Fish scales, carbonaceous detritus, and inoceramus molds are common along bedding planes. Calcareous pellets are rare.	0-6	Low diversity and diminutive suite Bed-by-bed fluctuation Common Lam-scram	*Planolites, Phycosiphon, Teichichnus, Nereites, Chondrites,* fugichnia	Prevalent storms (e.g., tempestites, WESGFs) with punctuating deltaic influence (e.g., hyperpycnites, ?wave-supported hyperpycnites) **Wave- and storm-influenced distal prodelta**	Fig. 5
3A	**Poorly to moderately bioturbated pinstriped medium grey silty mudstone**	Frequent siltstone starved current ripples and ripple-tail lamination. Common normally graded beds, rare wave rippled and low angle laminated siltstone beds. Bedding planes show common fish scales, rare ammonite and inoceramus molds. Bivalves and calcareous pellets are rare throughout.	0-5	Low diversity, diminutive suite Bed-by-bed fluctuation	*Planolites, Phycosiphon,* fugichnia	Prevalent wave action (e.g., WESGFs) punctuated by storms (e.g., tempestites) and deltaic influence (e.g., hyperpycnites) **Wave- and storm-influenced distal prodelta**	Fig. 6
3B	**Well bioturbated pinstriped medium grey silty mudstone**	Near complete biogenic homogenization obscures primary sedimentary features. Remnant starved ripples and ripple-tail lamination.	4-6	Difficult to tell burrow size and trace diversity Near complete homogenization over several beds (>20 cm thick) Overall 'fuzzy' appearance to reworked beds	*Planolites, Phycosiphon, Teichichnus, Cylindrichnus,* fugichnia	Similar setting to facies 3A, with less prevailing physicochemical stress (e.g., more intense biogenic reworking). Still under some wave-influence (e.g., WESGFs) **Storm-influenced shelf**	
4	**Moderately to well bioturbated silt-streaked dark grey mudstone**	Homogeneous-appearing dark grey mudstone beds predominate. Silt-streaked appearance owing to thin siltstone starved ripples and ripple-tail lamination. Some rippled structures show alternating silt and mud foresets. Bivalve fragments common throughout, calcareous pellets rare throughout, occasionally disaggregated and accumulated into starved ripple structures.	0-6	Low diversity and diminutive suite Bed-by-bed fluctuation Lam-scram reworking of silt beds (>5 mm thick) Near complete homogenization over relatively thick intervals (>10 cm)	*Planolites, Phycosiphon, Nereites, Chondrites,* fugichnia	Prevalent wave action (e.g., WESGFs) punctuated by weak storms (small tempestites and hyperpycnites) **Sediment-starved storm-influenced shelf**	Fig. 7
5	**Poorly to moderately bioturbated calcareous pinstriped dark grey mudstone**	Matrix composed of silt-sized mud aggregates, commonly occurring as re-transported intraclasts (Percy and Pedersen, 2020), calcareous pellets and muddy pelagic fecal pellets (Percy and Pedersen, 2020). Thin siltstone wave ripples, combined flow ripples, starved current ripples and ripple tail lamination, often capped by structureless-appearing mudstone beds. Sporadic normally graded beds and soft sediment deformation. Frequent bivalve fragments and bioclastic lags. Calcareous pellets commonly disaggregated and accumulated as starved ripples	0-6	Low diversity and diminutive suite Bed-by-bed fluctuation, some consistently reworked stacked beds 'fuzzy' appearance to more reworked beds	*Planolites, Phycosiphon, Teichichnus, Nereites,* fugichnia, navichnia IBF1	Prevalent wave action (WESGFs, winnowed sediments, disaggregated pellets, re-transported intraclastic aggregates) with punctuating storms (e.g., thin tempestites and hyperpycnites) **Sediment-starved storm-influenced shelf or prodelta fringe**	Fig. 8
6	**Poorly bioturbated silt-streaked calcareous dark grey mudstone**	Most calcareous facies, matrix dominated by sand and silt-sized mud aggregate composite particles (commonly as intraclasts) (Percy and Pedersen, 2020), bivalve fragments, and calcareous pellets. Homogeneous-appearing dark grey mudstone beds. Siltstone starved combined flow ripples, current ripples, and ripple-tail lamination. Rare to sporadic normally graded beds, flame structures at the base of starved ripples. Bioclastic lags are sporadic, while calcareous pellets are commonly disaggregated into starved ripple structures.	0-5	Poor lithologic contrast makes burrow identification difficult Bed-by-bed fluctuation Remnant bedding indicated near complete biogenic homogenization in certain instances	*Planolites, Phycosiphon, Palaeophycus,* fugichnia, navichnia	Prevalent wave action (winnowed sediments, disaggregated pellets, re-transported intraclastic aggregates, starved ripples) **Sediment-starved storm-influenced shelf under a high productivity water column**	Fig. 9

? represents a tentative identification.

RESULTS AND INTERPRETATIONS

Facies analysis

As this paper is focused on ichnological interpretation, conventional sedimentological and facies descriptions and ensuing interpretations are not included herein, but are summarised in Table 1 and Fig. 4 through Fig. 9.

The entire cored length reflects high degrees of heterogeneity and is thinly interbedded with grain size often shifting at millimetre intervals. Lithofacies were designated based on overall grain size and mineralogy, dominant sedimentary structures, bioturbation intensity and types of trace fossils. Terms 'rare', 'sporadic', 'common', 'abundant' and 'ubiquitous' are used to describe the increasing relative appearance of sedimentary and biogenic features. The terms 'interbedded', 'pin-striped' and 'silt-streaked' denote the common occurrence of silt beds >5 mm, 2 to 5 mm and <2 mm, respectively. Terms 'unbioturbated', 'poorly bioturbated', 'moderately bioturbated' and 'well bioturbated' were used to denote BIs 0, 1 to 3, 3 to 4 and >5, respectively.

Seven lithofacies are recognised (Table 1, Figs 4 to 9). As this is an ichnologically focused study, descriptive facies names are used for ease of understanding as opposed to the standardised facies naming scheme for mudstones proposed by Lazar *et al.* (2015b). Facies include: (1) interbedded normally graded and silt rippled medium grey silty mudstone, (2) poorly to moderately bioturbated interbedded rippled silt and medium grey mudstone, (3A) poorly to moderately bioturbated pinstriped medium grey silty mudstone, (3B) well-bioturbated pinstriped medium grey silty mudstone, (4) poorly to well-bioturbated silt-streaked dark grey mudstone, (5) poorly to moderately bioturbated calcareous pinstriped dark grey mudstone and (6) poorly bioturbated silt-streaked calcareous dark grey mudstone.

Overall, cursory facies interpretations indicate varying deltaic, storm and wave influence through time under relatively shallow waters (<70 m, above storm wave base). Facies are

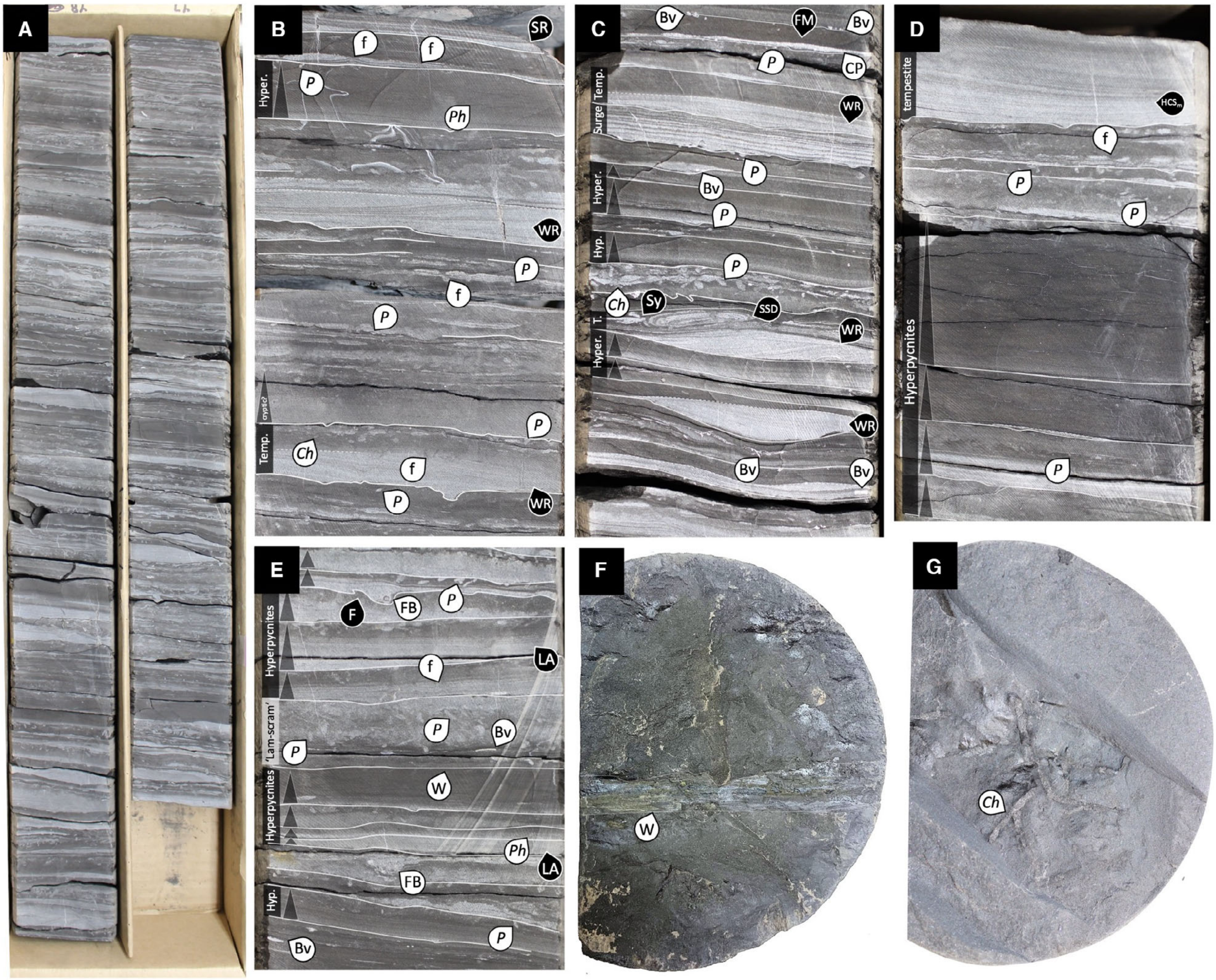

Fig. 4. Core photographs showing variation within Facies 1. (A) Representative box core of Facies 1 (2801.70 to 2800.35 m). (B) Photograph showing bed-by-bed fluctuation of bioturbation within the facies, and top-down 'lam-scram' reworking of several beds (2807.25 m). (C) Photograph showing diverse heterogeneity of facies, with stacked hyperpycnites and tempestites (2804.35 m). (D) Thick stacked muddy hyperpycnites and base of overlying thick tempestite (2805.80 m). (E) Stacked hyperpycnites with intervening top-down bioturbated beds (2806.95 m). (F) Wood fragment along bedding plane (2789.20 m). (G) Silt-filled *Chondrites* burrow network (2805.65 m). White labels represent biologic features and black labels represent sedimentological features. White abbreviations: *P* (*Planolites*), *Ph* (*Phycosiphon*), *Ch* (*Chondrites*), f (fugichnia), Bv (bivalve), CP (calcareous pellets), FB (fish bones) and W (wood fragment). Black abbreviations: SR (starved ripple), WR (wave ripple), LA (low angle lamination), F (flame structure), Sy (syneresis), SSD (soft sediment deformation) and HCSm (micro-hummocky cross stratification). Bold white lines represent bedding contacts, dashed white lines represent internal bed boundaries. Grey triangles represent graded intervals. Core is 7 cm in diameter.

numbered from most proximal (e.g. Facies 1) to most distal (e.g. Facies 6), representing decreasing energy levels with increasing distance from the western palaeoshoreline.

Ichnology

Previous studies of the Canadian OAE2-bearing interval have characterised it as largely devoid of burrowing (e.g. Bloch *et al.*, 1993), or poorly to moderately bioturbated with only a few distinct ichnogenera (Hosseininejad Mohebati, 2016; Percy & Pedersen, 2020). The ichnological analysis presented here reveals a higher diversity of ichnogenera and generally increased bioturbation intensities compared to earlier assessments, a difference attributed to the finer scale of investigation employed. The

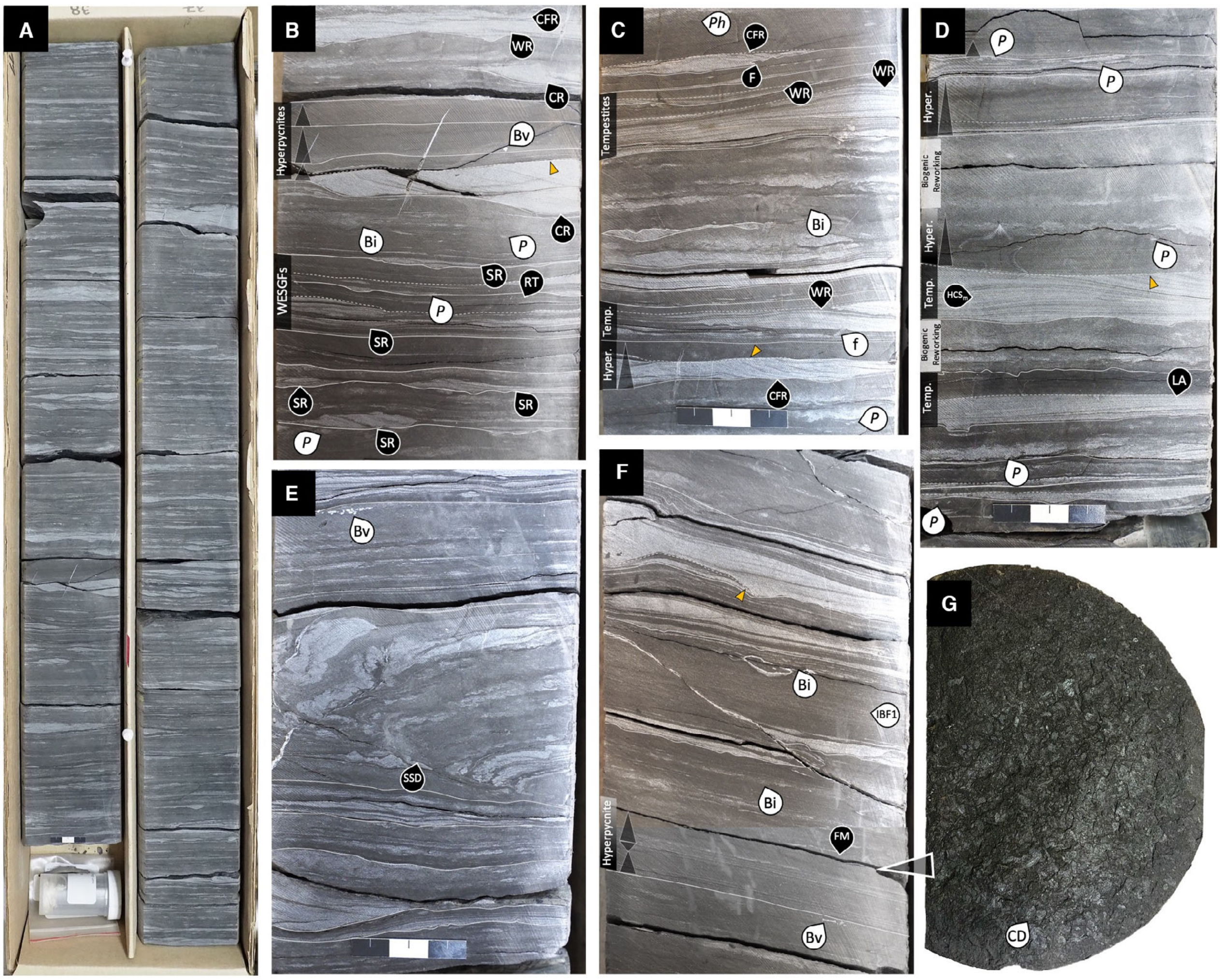

Fig. 5. Core photographs showing variation within Facies 2. (A) Representative box core photograph of Facies 2 (2738.20 to 2736.70 m). (B) Core photograph showing variation in silt ripple types, and contrasting WESGF and hyperpycnite beds (2737.95 m). (C) Photograph showing bed-by-bed fluctuating intensities of biogenic reworking (2735.15 m). (D) Photograph showing hyperpycnites and tempestites, with intervening bioturbation (2743.35 m). (E) Relatively large-scale soft sediment deformation (2741.55 m). (F) Homogeneous-appearing dark mudstone beds with intervening silt ripples (2755.20 m). (G) Carbonaceous detritus on bedding plane in (F). White labels represent biologic features and black labels represent sedimentological features. White abbreviations: *P* (*Planolites*), Bi (bioturbation), IBF1 (inconspicuous bioturbated fabric 1), Bv (bivalve) and CD (carbonaceous detritus). Black abbreviations: SR (starved ripple), WR (wave ripple), CFR (combined flow ripple), CR (current ripple), LA (low angle lamination), F (flame structure), HCS (hummocky cross-stratification) and SSD (soft sediment deformation). Bold white lines represent bedding contacts, dashed white lines represent internal bed boundaries. Grey triangles represent graded intervals. Yellow arrows denote scour surfaces. Core is 7 cm in diameter.

total ichnological dataset over the cored interval is illustrated in Fig. 10.

Burrows are documented nearly exclusively in elevation view (on clean slabbed core faces). Bioturbation is identified most clearly in intervals of high lithologic contrast (e.g. intercalated siltstone and mudstone beds) where passive and active silty-sediment infilling of burrows in mudstone beds, or emplacement of mud-filled or mud-lined burrows in lighter coloured silty beds leads to high contrast duochromatic structures (e.g. Fig. 10). Bioturbation is also commonly recognised as top-down reworking ('lam-scram') of coarser grained (silt-mineral dominated) beds, where primary sedimentary structures are preserved at the base of the bed, below the penetration extents of burrows (e.g. Figs 4B to E, 5D, 6G and 7E). In low contrast areas (i.e. stacked beds

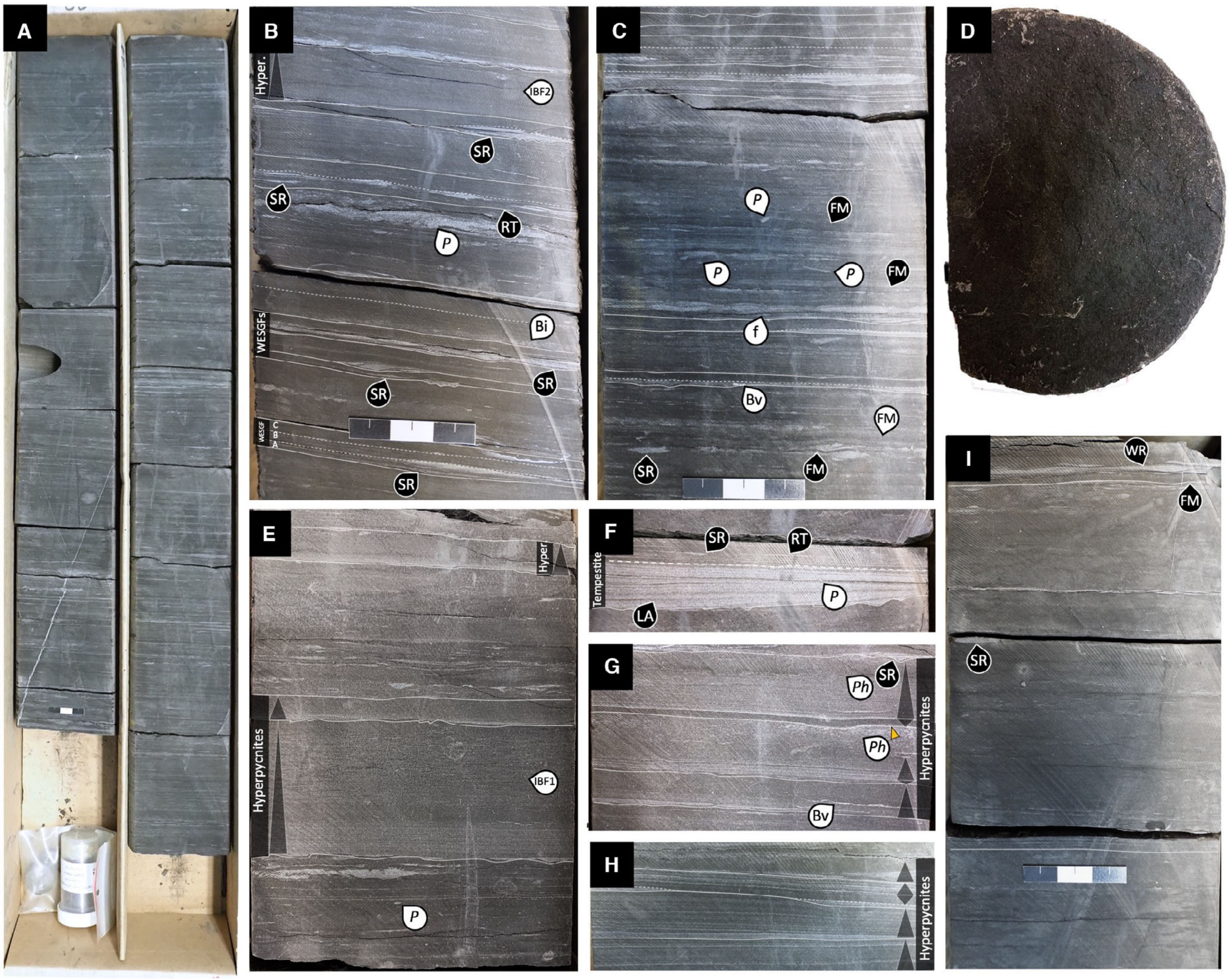

Fig. 6. Core photographs of variation within Facies 3A (B-H) and 3B (I). (A) Representative box core photograph (2727.00 to 2725.75 m). (B) Photograph of pin-striped appearance resulting from starved ripples. Stacked bedsets of starved ripples up through structureless mudstones represent WESGFs. Internal tripartite structure denoted by A, B and C labels (e.g. Macquaker *et al.*, 2010). (C) Partially bioturbated pin-striped starved silt ripple interval (2726.20 m). (D) Macerated fish scales resulting in a sparkly appearance along bedding planes (2698.90 m). (E) Stacked hyperpycnites in otherwise pin-striped mudstones (2708.05 m). (F) (2698.15 m), (G) (2704.70 m) and (H) (2729.95) showing various appearance of normally graded hyperpycnites. (G) Uppermost hyperpycnite shows basal mud layer emplaced during waxing phase. (I) Representative core photograph of the well-bioturbated Facies 3B (2731.65 m). White labels represent biologic features and black labels represent sedimentological features. White abbreviations: *Ph* (*Phycosiphon*), *P* (*Planolites*), f (fugichnia), IBF1 (inconspicuous bioturbated fabric 1), IBF2 (inconspicuous bioturbated fabric 2), FS (fish scales) and Bv (bivalve). Black abbreviations: RT (ripple tail), SR (starved ripple), WR (wave ripple), LA (low angle lamination) and FM (fluid mud). Grey triangles represent graded intervals. Yellow arrows denote scour surfaces. Core is 7 cm in diameter.

of similar lithology and/or colour) where discrete trace fossils are not always clear, bioturbation results in beds with diffuse bounding margins (bedding contacts are not obvious), interrupted otherwise continuous laminae (e.g. laterally punctuated laminae), and an overall 'fuzzy' appearance (e.g. Figs 4B, 5D and 8G) (e.g. Schieber *et al.*, 2021; Biddle *et al.*, 2025).

Ichnogenera diversity, trace fossil diameters and extent of biogenic reworking (i.e. Bioturbation Index) show constant fluctuation over the length of this core, often on a bed-by-bed scale. A total of nine distinct trace fossil types are identified herein. The maximum diversity recorded for a single 10 cm bin was five types. Burrow diameters range between 1 mm and

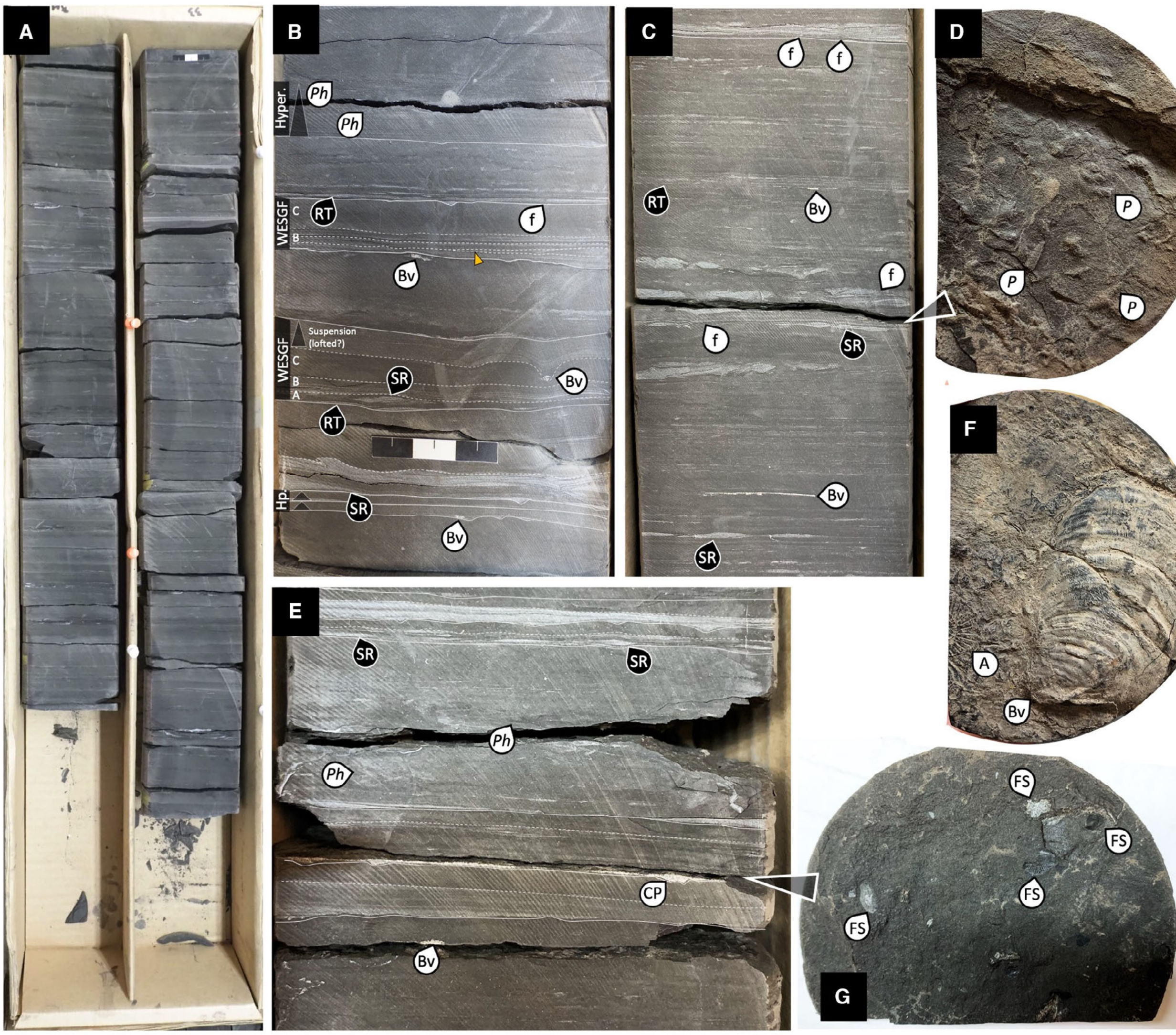

Fig. 7. Core photographs of variation within Facies 4. (A) Representative core box photograph (2704.75 to 2703.60 m). (B) Well-bioturbated dark grey mudstone with intercalated WESGFs and hyperpycnites (2723.85 m). (C) Representative silt-streaked appearance (2725.60 m). (D) *Planolites* along bedding plane in (C). (E) Starved silt-mineral ripples and calcareous pellet lags (2718.70 m). (F) Inoceramous bivalve and small ammonite mould (2729.75 m). (G) Fish scales along bedding plane in (E). White labels represent biologic features and black labels represent sedimentological features. White abbreviations: *Ph* (*Phycosiphon*), *P* (*Planolites*), f (fugichnia), Bi (bioturbation), CP (calcareous pellets), FS (fish scales), Av (bivalve) and a (ammonite). Black abbreviations: RT (ripple tail) and SR (starved ripple). Yellow arrows denote scour surfaces. All core is 7 cm in diameter.

6 mm, most commonly being between 1 mm and 3 mm. The largest recorded burrows, having 6 mm diameters, were only noted in 10 bins, accounting for <1% of the cored interval. The only tiering relationship identified in this core is that of occasional microscopic bioturbation overprinting macroscopic traces (identified petrographically).

The small size and lack of bedding plane orientations restrict ichnotaxa identification to the ichnogeneric level. The seven ichnogenera identified throughout this core include: (i) fully marine specialised deposit feeding traces of *Phycosiphon* and *Nereites*, (ii) the fully marine specialised deposit feeding and chemosymbiotic traces of *Chondrites*, (iii) eurytopic deposit feeding traces of *Planolites* and *Teichichnus* and (iv) the dwelling, filter feeding or predation traces of *Cylindrichnus* and *Palaeophycus*. Fugichnia (i.e. 'escape traces') are also observed throughout.

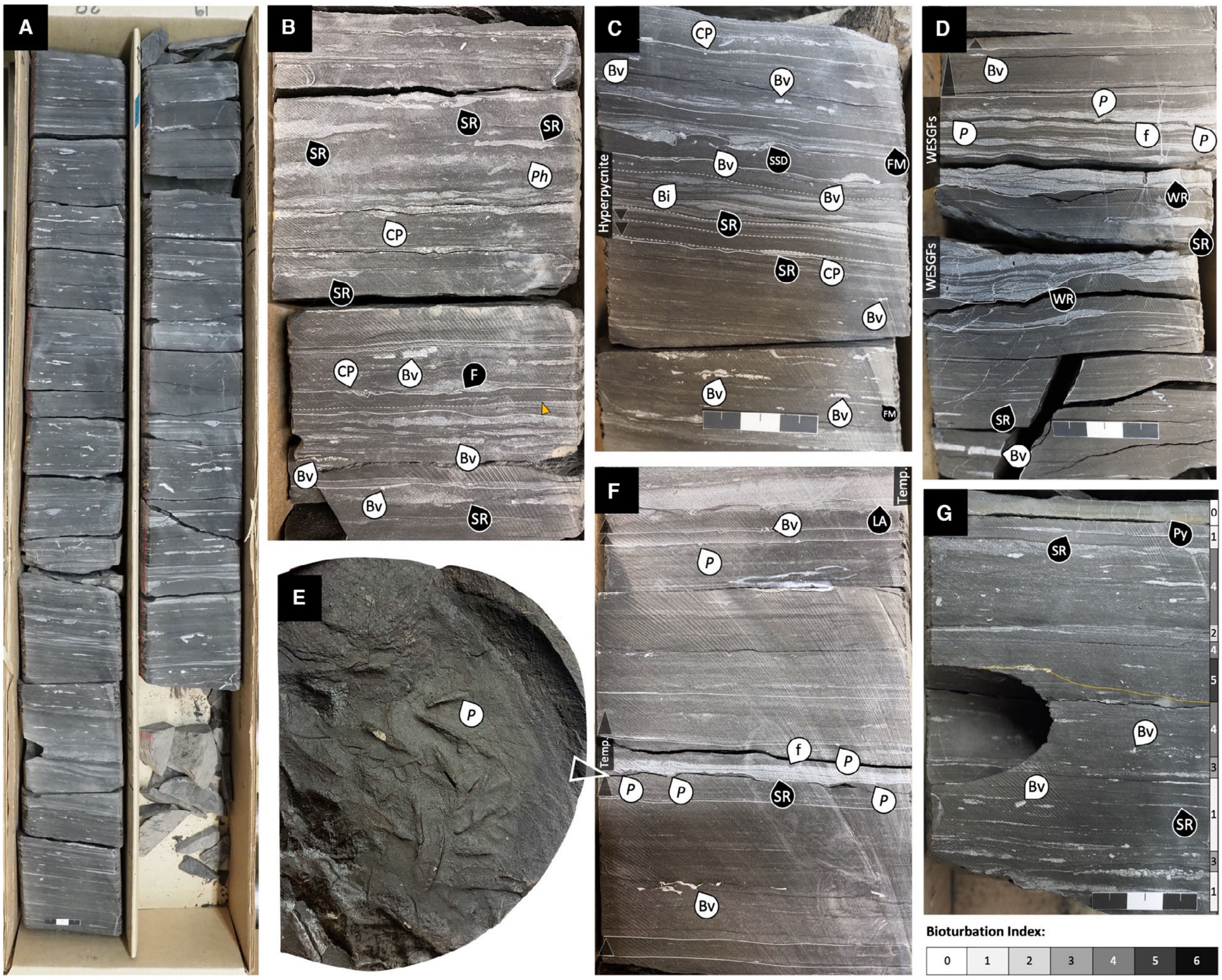

Fig. 8. Core photographs showing variation within Facies 5. (A) Representative box core of Facies 5 (2754.70 to 2753.45 m). (B) Photograph showing moderately bioturbated character with calcareous pellets and common bivalve fragments (2746.35 m). (C) Poorly bioturbated starved rippled pin-striped interval (2754.35 m). (D) Starved rippled dark grey mudstone with stacked WESGFs (2760.90 m). (E) *Planolites* along bedding plane in (F). (F) Pin-striped appearance with thin normally graded beds and thin silt-mineral ripples (2787.65 m). (G) Representative photograph showing the subtlety of bioturbation variation. Coloured bars to the right indicate BI. Orange line illustrates the boundary between a well bioturbated overlying bed and a weakly bioturbated bed with preserved lamination below (2781.60 m). White labels represent biologic features, black labels represent sedimentological features. White abbreviations: *P* (*Planolites*), f (fugichnia), Bv (bivalve) and CP (calcareous pellets). Black abbreviations: SR (starved ripple), WR (wave ripple), LA (low angle lamination), FM (fluid mud), F (flame structure), SSD (soft sediment deformation) and Py (pyrite). Bold white lines represent bedding contacts and dashed white lines represent internal bed boundaries. Grey triangles represent graded intervals. Yellow arrows denote scour surfaces. Core is 7 cm in diameter.

Occurrences of ichnogenera are displayed in Fig. 10. Detailed descriptions and occurrences of ichnogenera can be found in Data S1 and Fig. 11.

Macroscopic 'fuzzy' appearances of beds or internal laminae are attributed to varying degrees of reworking by infaunal meiofauna (e.g. Schieber & Wilson, 2021); subsequently confirmed by thin-section analysis (Figs 12 and 13). Extents of meiofaunal reworking vary bed-by-bed, and even within a single bed (e.g. Fig. 14). In many cases, meiofaunal reworking is most intense near the tops of beds, leaving the depositional character of the bases preserved (e.g. Fig. 12); mimicking that of macroscopic 'lam-scram' textures. Many beds that appear macroscopically as unbioturbated (e.g. Fig. 12C), show evidence of meiofaunal reworking in thin-section (e.g. Fig. 12D).

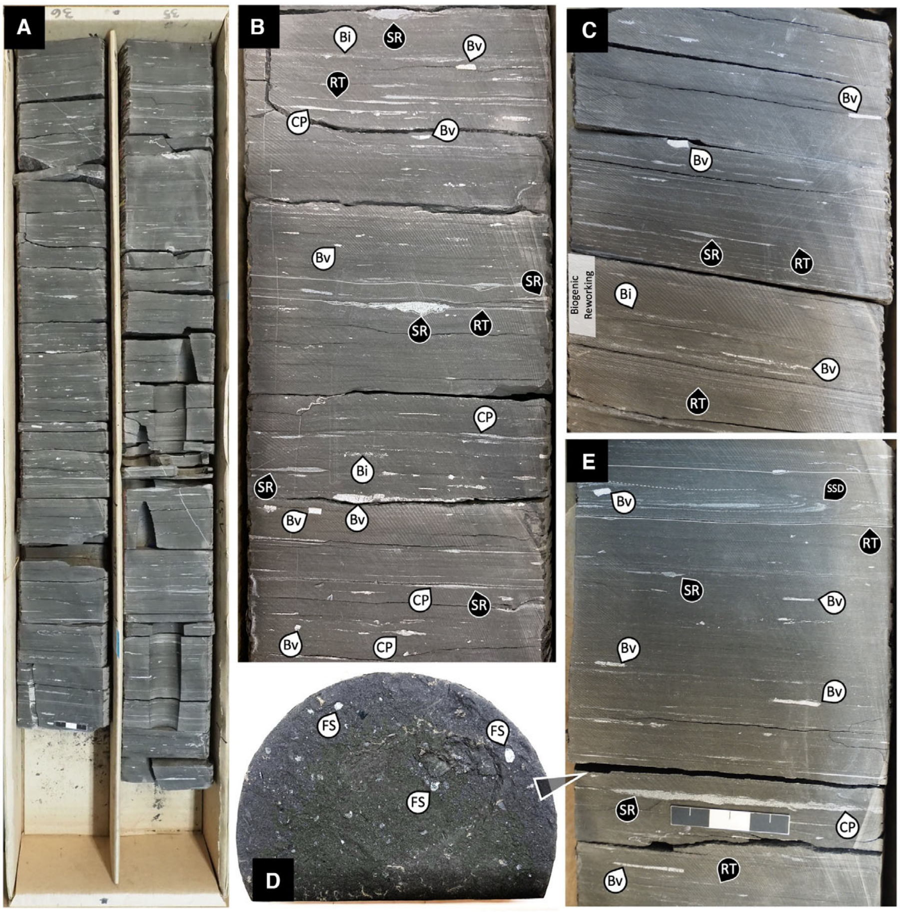

Fig. 9. Core photographs showing variation within Facies 6. (A) Representative box core of Facies 6 (2765.10 to 2763.75 m). (B) Photograph showing silt-streaked appearance of calcareous pellets (2764.70 m). (C) Photograph showing that 'silt streaks' are likely the product of ripple tail lamination (2757.25 m). (D) Fish scales along bedding plane in (E), resulting in sparkly appearance. (E) Silt-streaked mudstone with soft sediment deformation near top and calcareous pellet lag above scale bar (2761.10 m). White labels represent biologic features and black labels represent sedimentological features. White abbreviations: Bv (bivalve), CP (calcareous pellets) and Bi (bioturbation). Black abbreviations: SR (starved ripple), RT (ripple tail lamination) and SSD (soft sediment deformation). Bold white lines represent bedding contacts and dashed white lines represent internal bed boundaries. Core is 7 cm in diameter.

Additionally, three indistinct biodeformational fabrics (IBFs) are noted. These include: (i) compacted burrowed medium-grey-coloured mudstones; (ii) homogeneous-appearing dark-grey mudstones; and (iii) 'mantle and swirl' traces (navichnia; i.e. 'sediment swimming' traces). Superficially laminated compacted burrowed medium-grey mudstones (IBF1), which contain dark-grey wavy streaks often mistaken for organomineralic aggregates or mud intraclasts, are confirmed by thin-section analysis to instead represent a 'burrow-laminated' fabric formed by the compaction of dominantly horizontal bioturbation structures (Figs 5F, 6E and 14). Homogeneous-appearing dark-grey mudstones (IBF2) appear similar to dark-grey structureless fluid mud beds but show faint remnant heterogeneity with diffuse borders (Figs 6B and 15). This faint heterogeneity is more obvious in thin sections (Fig. 12C,D). These beds are taken to represent near-complete biogenic homogenisation. More detailed descriptions of these biodeformational fabrics can be found in Data S1.

Ichnofacies

The bed-by-bed alternation of bioturbation intensity, the overall diminutive and impoverished trace fossil suites, the presence of

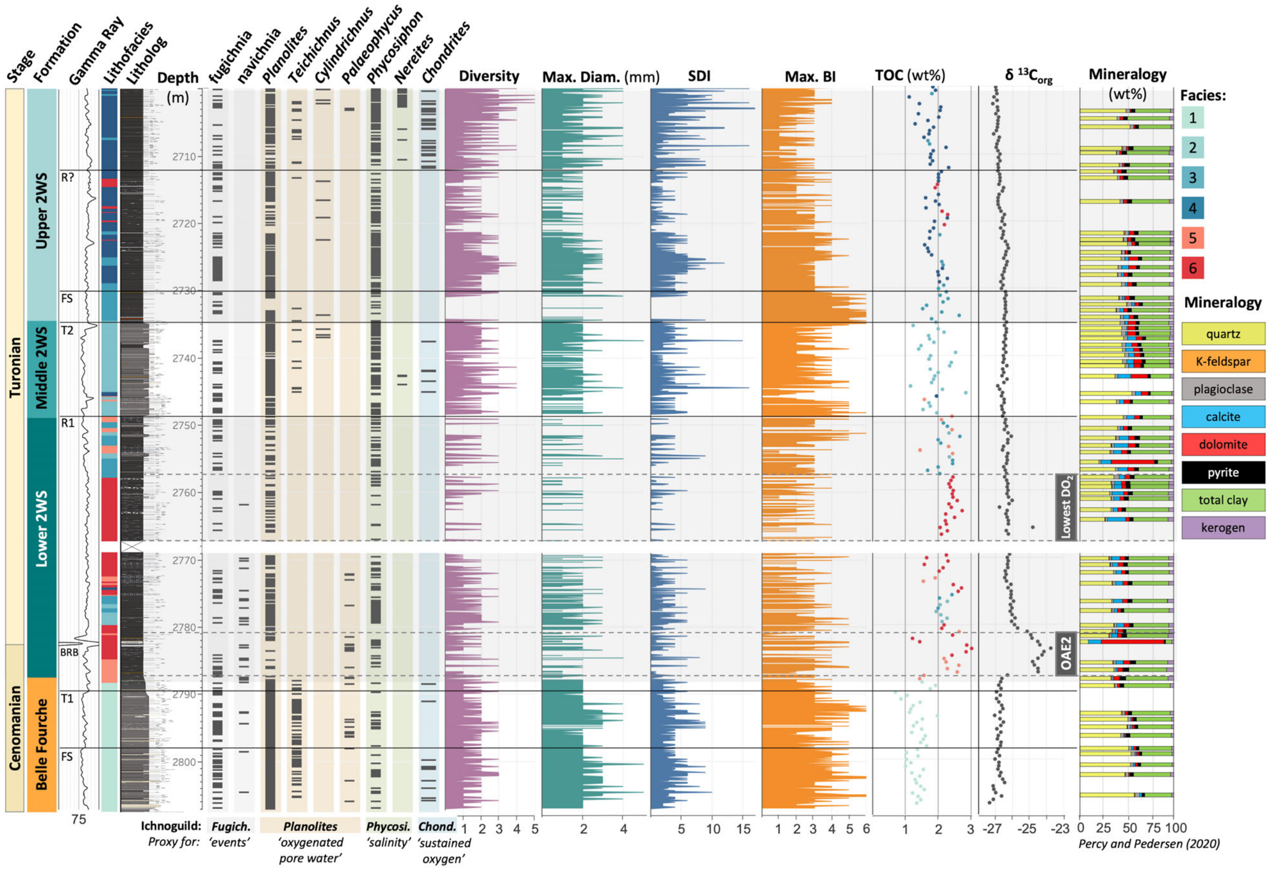

Fig. 10. Facies, ichnologic data, TOC (wt%), carbon isotopes and mineralogy distributions over the entire cored interval. Ichnogenera organised by their ichnoguild association (coloured bars match colours in Table 2). Mineralogy from XRD analysis of Percy & Pedersen (2020). Stratigraphic surfaces from Percy (2021), regressive 'R', transgressive 'T', flooding surface 'FS', Bighorn River Bentonite 'BRB'. 'R?' indicates a new surface Ichnologically identified herein.

common navichnia in the lower section and the predominance of *Phycosiphon* and fugichnia throughout make this entire core analogous to MacEachern & Bann's (2020) recently proposed *Phycosiphon* Ichnofacies. Characterising the entire core length as belonging to the *Phycosiphon* Ichnofacies limits a more detailed understanding of small-scale variations in physicochemical conditions. Therefore, the ichnological data have been further subdivided into distinct ichnoguilds.

Ichnoguilds

An ichnoguild is a behavioural ordering system defined as a group of organisms that use similar feeding strategies to exploit a shared tier (e.g. depth) below the sediment–water interface (Bromley, 1996). Three main parameters are considered when defining an individual ichnoguild: (i) the temporal occupancy of a burrow; (ii) the food resource being exploited; and (iii) the depth of exploitation (Bromley, 1996). The temporal occupancy of a burrow is categorised as either permanent/semi-permanent (e.g. dwelling structures, sessile organisms), or transient (e.g. mobile feeding structures) (Bromley, 1996; Buatois & Mangano, 2003). Exploited food resources include detritus or deposit feeding, suspension feeding and chemosymbiosis (Bromley, 1996). Depth of exploitation refers to the depth of the sediment tier being exploited, for example, shallow-tier or deep-tier. Similar to Seilacherian Ichnofacies, ichnoguilds are named based on the dominant ichnotaxon (Bromley, 1996; Buatois & Mangano, 2003).

Four distinct ichnoguilds are identified herein: (i) the fugichnia ichnoguild, (ii) the

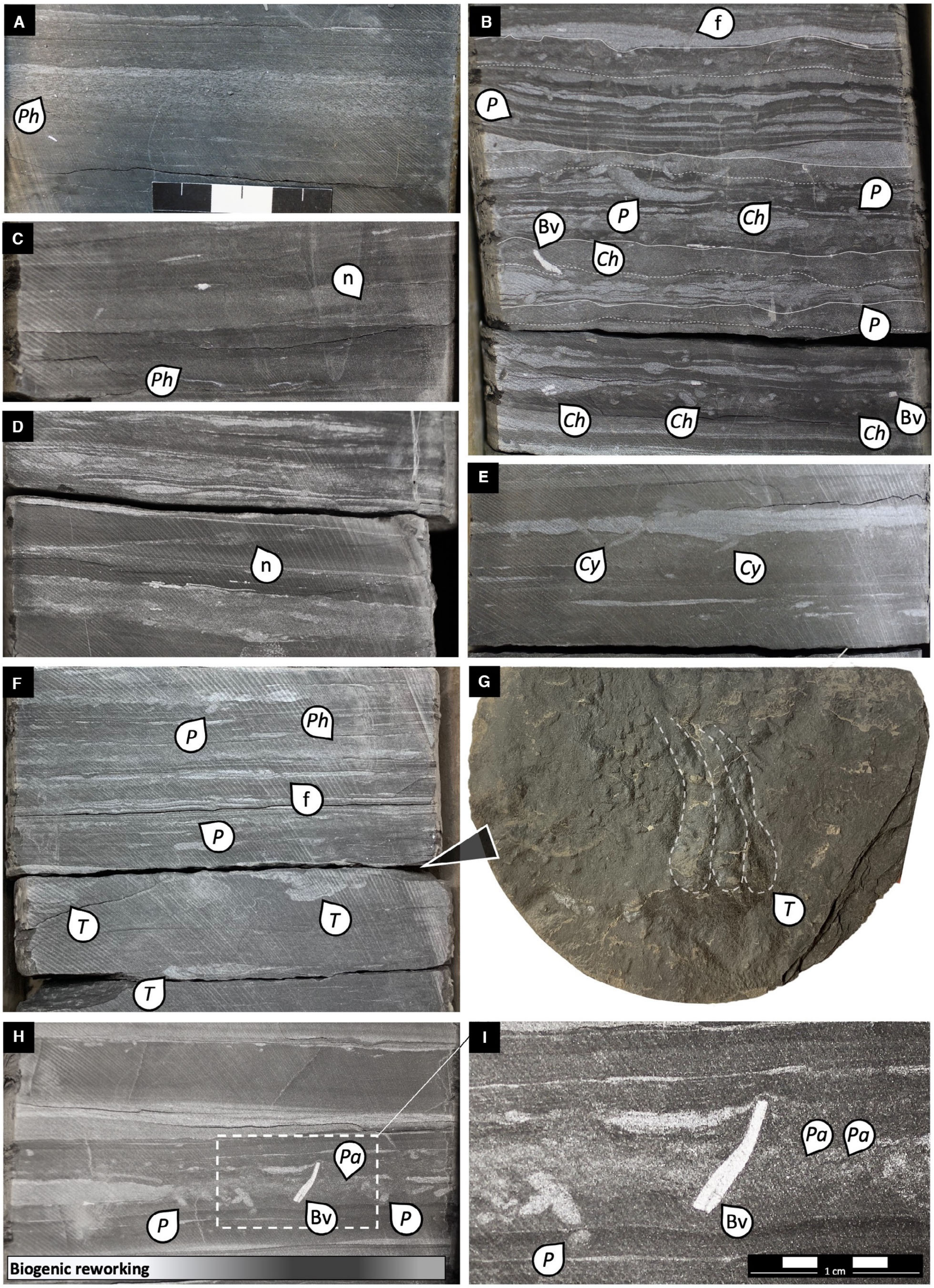
A
Ph
B
f
P
P
Bv
P
Ch
Ch
P
Ch
Ch
Ch
Bv
C
n
Ph
D
n
E
Cy
Cy
F
P
Ph
f
P
T
T
T
G
T
H
Pa
P
Bv
P
Biogenic reworking
I
Pa
Pa
Bv
P
1 cm

Fig. 11. Expression of Ichnological features of the Bell Fourche and Second White Specks Formations. (A) *Phycosiphon* colonising silty beds (2703.75 m). (B) *Planolites* most easily seen in dark mud beds, and *Chondrites* exclusively occurring in dark grey mud beds (2798.56 m). Solid white lines denote individual sedimentation events, extent of top-down reworking of bedsets (lam-scram) marked by dashed lines (2800.35 m). (C) A single navichnia occurrence in a silty bed, *Phycosiphon* in silty bed below (2784.61 m). (D) Navichnia (sediment swimming trace) seen in dark mud (fluid mud). (E) Several *Cylindrichnus* penetrating underlying mud bed (2710.63 m). (F) Large *Teichichnus* in mud bed (largest trace diameter documented in the entire core length), small fugichnia seen in thin silt bed, *Phycosiphon* fully reworking a silt bed, small *Planolites* throughout (2741.40 m). (G) Bedding plane view of *Teichichnus* in (F) (right-side outlined). (H) Central bed showing the lateral variability of biogenic reworking, illustrated in the gradient bar along the bottom (2794.74 m). (I) Close-up photograph of outlined area in (H) showing mm scale *Palaeophycus* burrows. Abbreviations: *Phycosiphon* (*Ph*), *Planolites* (*P*), *Chondrites* (*Ch*), *Zoophycos* (*Z*), *Cylindrichnus* (*Cy*), *Teichichnus* (*T*), *Palaeophycus* (*Pa*), navichnia (n), fugichnia (f) and bivalve fragment (bv). All core is 7 cm in diameter.

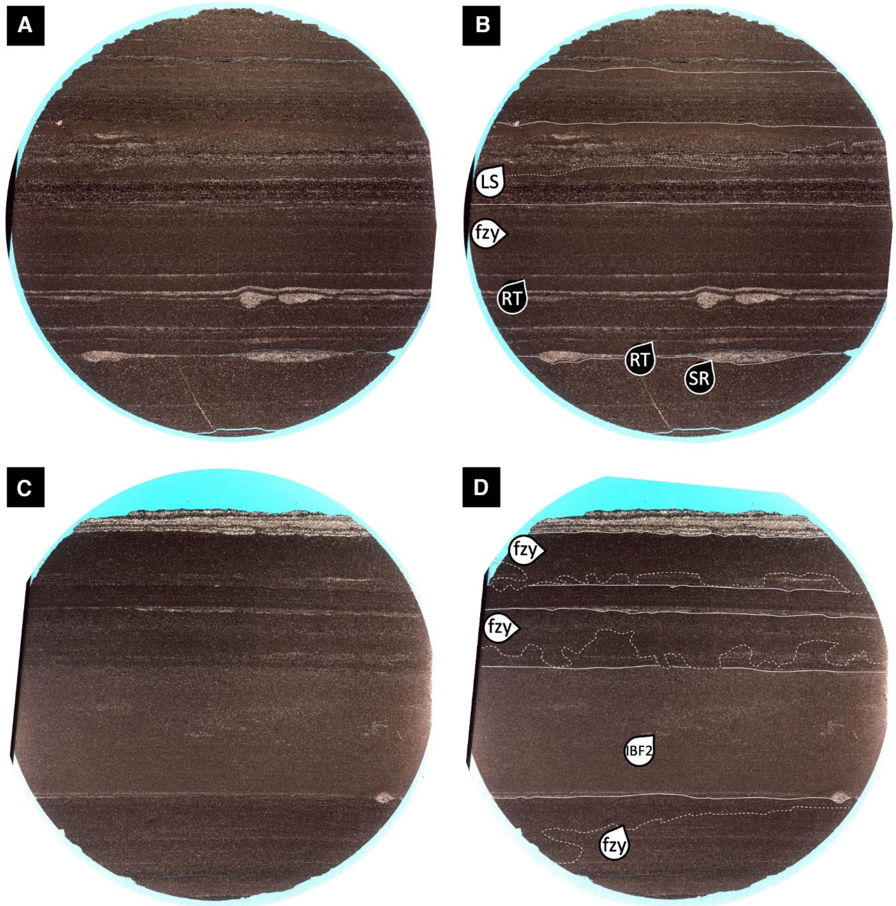

Fig. 12. Photomicrographs illustrating the utility of microichnological analysis. (A) Thin section showing well-laminated appearance (2758.75 m). (B) Annotated image from (A) outlining signs of meiofaunal reworking, both as lam-scram (top-down; LS) reworking of beds and an overall fuzzy appearance (fzy). (C) Thin section showing well-defined beds (2787.20 m). (D) Annotated image from (C) outlining the fuzzy top-down reworking of beds (fzy), as well as remnant heterogeneity within an otherwise biogenically homogenised bed (IBF2). Standard thin section diameters (2 cm).

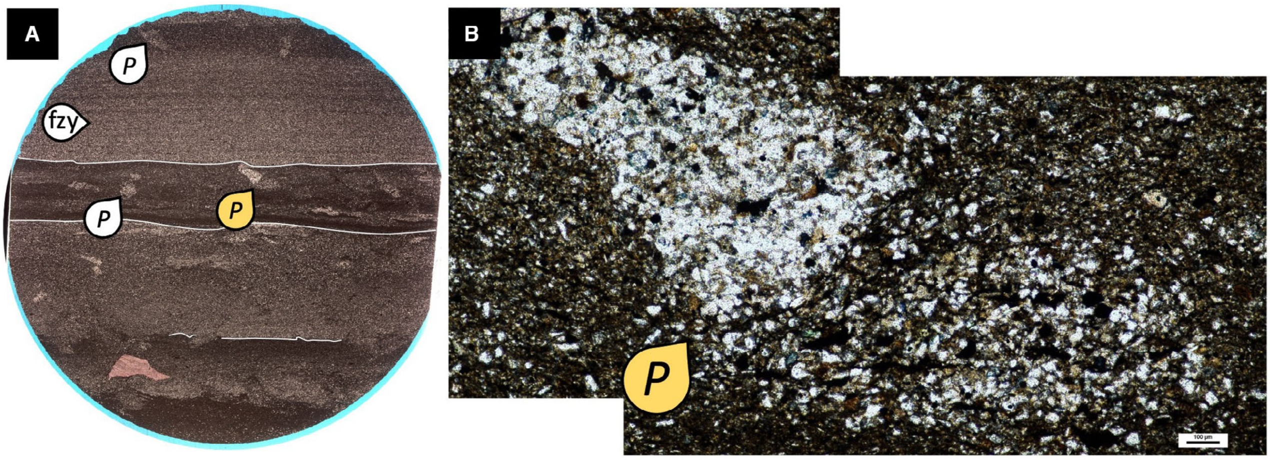

Fig. 13. Example of meiofaunal overprinting. (A) Thin section scan showing macroscopic silt-filled *Planolites* (*P*). Uppermost normally graded bed is also cryptically bioturbated, resulting in an overall 'fuzzy' appearance. Standard thin section (2 cm diameter) (2793.45 m). (B) Photomicrograph mosaic showing partial meiofauna reworking of a single *Planolites* (yellow label in both figures). Base of trace appears fuzzy and homogenised due to meiofaunal grain reorganisation. Scale bar: 100 µm.

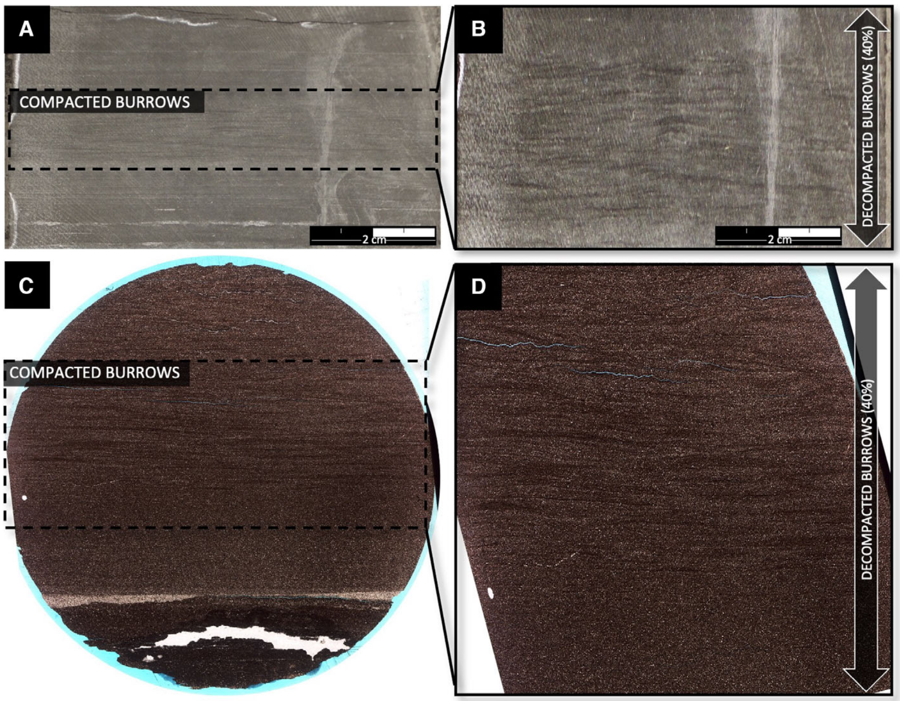

Fig. 14. Core photographs and photomicrograph of burrows within compacted medium grey muds, termed inconspicuous bioturbated fabric 1 (IBF1). (A) Core photograph showing wispy darker grey features within an otherwise homogeneous-appearing medium grey mudstone bed (2787.70 m). Core is 7 cm in diameter. (B) Virtually 'decompacted' mud bed, where photograph was vertically stretched to show likely sediment character prior to 40% dewatering (e.g. Schieber, 2003). (C) Photomicrograph of erosive based compacted plug-like fluid mud showing top-down colonisation by obscure traces of IBF1 (2745.60 m). Thin section is 2 cm in diameter. (D) Virtually decompacted image (to 40% dewatering), enhancing original non-parallel orientation and same matrix fill.

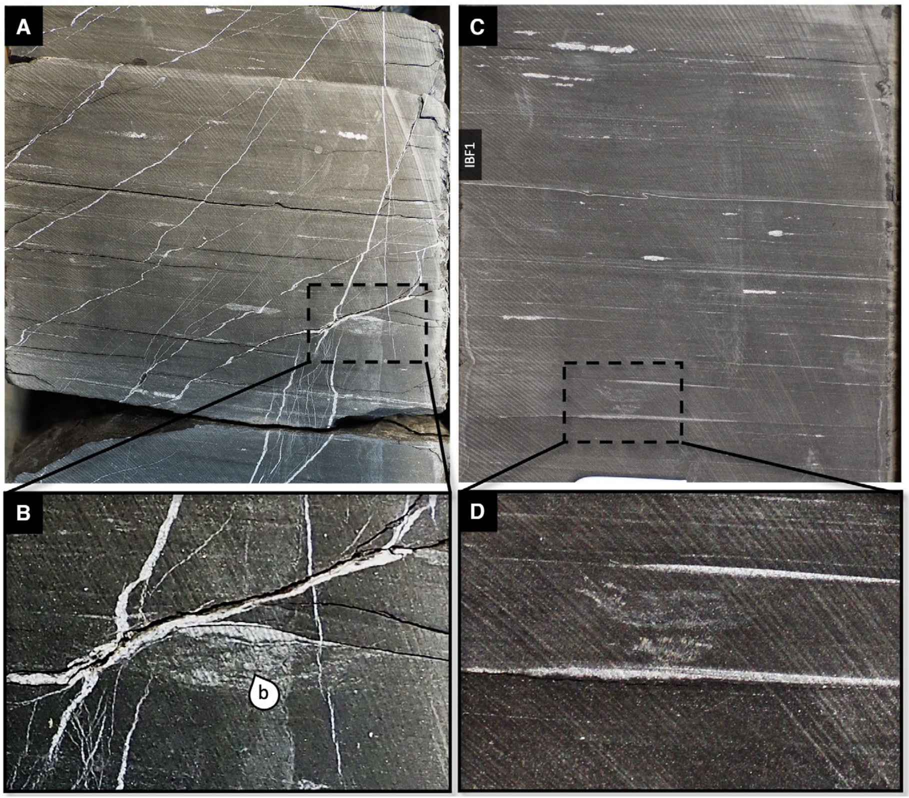

Fig. 15. Core photographs of remnant heterogeneity in nearly fully biogenically homogenised mud beds (IBF2). (A) Core photograph showing poor lithologic contrast in dark mudstone interval. Small remnant silt bed seen in outlined area (2761.50 m). (B) Digitally enhanced (sharpened, increased colour contrast) remnant silt bed from (A) showing small circular burrows (b). (C) Subtle remnant heterogeneity of IBF2 (dashed outline). IBF1 occurs in a bed near the top of the photograph (2783.70 m). (D) Enhanced bed from (C). Core in (A) and (C) is 7 cm in diameter.

Planolites ichnoguild, (iii) the *Phycosiphon* ichnoguild and (iv) the *Chondrites* ichnoguild (summarised in Table 2).

Fugichnia ichnoguild

The fugichnia ichnoguild (grey ichnogenera columns in Fig. 10) is characterised by mobility traces that are not associated with specific feeding patterns or ichnotaxa, and consists of fugichnia and navichnia. This ichnoguild provides a line of depositional evidence, rather than insights into tiering relationships and resource exploitation. Fugichnia are animal escape structures, indicating rapid sediment emplacement. Navichnia records a sediment-swimming behaviour as organisms migrate through soupy muds. Although both trace fossils are typified by different event deposits, their existence indicates rapid and episodic sedimentation and can act as a visual proxy for episodic sedimentation on Fig. 10. Navichnia may also signal a delta-proximal position, where river-derived fluid muds can propagate via wave/storm resuspension and enhancement.

Planolites ichnoguild

The *Planolites* ichnoguild (orange ichnogenera columns in Fig. 10) is characterised by shallow tier deposit feeding structures created by both mobile and sessile organisms. Compositional ichnotaxa include *Planolites*, *Teichichnus*, *Palaeophycus* and *Cylindrichnus*. These traces dominantly reflect the behaviours of facies-crossing trophic generalists (e.g. Gingras *et al.*, 2007) and are common of organisms able to withstand reduced salinity (e.g. Howard & Frey, 1973, 1975; Howard *et al.*, 1975; Gingras *et al.*, 1999, 2011; Buatois *et al.*, 2005; MacEachern & Gingras, 2007; Dashtgard *et al.*, 2008). Further, *Planolites* represents backfilled grazing traces (i.e. no connection to the sediment–water interface), and as such the burrowing animals likely fulfilled their dissolved oxygen requirements from surrounding non-anoxic pore-waters.

Table 2. Ichnoguild characteristics. Colours correspond to those seen in Figs 10 and 16.

Ichnofacies	Ichnoguild	Ichnogenera	Temporal Occupancy	Feeding Strategies	Environment	Proxy for
Phycosiphon	Fugichnia	Fugichnia	Transitory (mobile)	N/A – Escape structure	Rapidly deposited sediment	Episodic sedimentation
		Navichnia	Transitory (mobile)	N/A – Sediment swimming structure	Soupy substrate (fluid mud)	
	Planolites	*Planolites*	Transitory (mobile)	Deposit feeding	Shallow tier, marine or freshwater influence	Oxygenated pore waters
		Palaeophycus	Permanent/ semi-permanent (sessile)	Deposit feeding/ carnivory	Shallow tier, fully marine or fresh water influence	
		Teichichnus	Semi-permanent (sessile)	Surface detritus feeding, deposit feeding	Shallow tier, fully marine or fresh water influence	
		Cylindrichnus	Permanent	Surface detritus feeding	Shallow tier, fully marine or fresh water influence, opportunistic	
	Phycosiphon	*Phycosiphon*	Transitory (mobile)	Deposit feeding	Shallow tier, fully marine, opportunistic	Normal marine salinity
		?Nereites	Transitory (mobile)	Deposit feeding, surface grazing	Shallow tier, fully marine or fresh water influence	
	Chondrites	*Chondrites*	Permanent/ semi-permanent (sessile)	Deposit feeding	Middle-deep tier, fully marine or freshwater influence, oxygen stress	Sustained oxygenated bottom waters

? represents a tentative identification.

Overall, the generalist elements of the *Planolites* ichnoguild do not reflect characteristics signalling specific conditions beyond that of non-anoxic pore-waters at the time of burrow emplacement. Distributions of the *Planolites* ichnoguild in Fig. 10 may act as a visual proxy for (at least temporarily) oxygenated pore waters.

Phycosiphon ichnoguild

The *Phycosiphon* ichnoguild (green ichnogenera columns in Fig. 10) is characterised by generally fully marine (i.e. normal salinity) shallow-tier specialised mobile deposit feeders of *Phycosiphon* and shallow-tier deposit feeders and surface grazers of *Nereites* (e.g. Goldring *et al.*, 1991; Wetzel & Bromley, 1994; Bednarz & McIlroy, 2009; Gingras *et al.*, 2011; Rodríguez-Tovar & Dorador, 2014; Comerio *et al.*, 2018; MacEachern & Bann, 2020). *Phycosiphon* is a known rapid opportunistic coloniser of event beds (Wetzel & Uchman, 2001). Thus, its relative absence in the event-bed-dominated Belle

Fourche Formation (i.e. Facies 1) indicates salinity fluctuations play a dominant role in dictating the occurrences of this ichnoguild. Much like *Planolites*, *Phycosiphon* does not maintain an open connection to the sediment–water interface, requiring bioavailable DO_2 in pore waters (Wetzel & Uchman, 2001). Ultimately, the occurrence of this ichnoguild signals fully marine depositional conditions (e.g. euryhaline) in sediments with oxygenated pore waters. The strong association of *Phycosiphon* and *Nereites* herein to fully marine conditions (e.g. euryhaline) allows this ichnoguild to act as a visual proxy for normal marine salinity in Fig. 10.

Chondrites ichnoguild

The *Chondrites* ichnoguild (blue ichnogenera columns in Fig. 10) represents specialised deep-tier permanent deposit-feeding and/or chemosymbiotic structures of exclusively *Chondrites*. These deep-tier permanent organisms are controlled by the availability of oxygen in bottom waters rather than that of sediment pore waters (e.g. Bromley & Ekdale, 1984; Ekdale & Mason, 1988; Smith *et al.*, 2000; Martin, 2004), as trace makers maintain an open connection to the sediment–water interface allowing irrigation of oxygenated waters at depth. The redox potential discontinuity (RPD) will shallow within the sediments if pore water oxygen concentrations are low, constricting the depths to which mobile deposit feeders can penetrate (Bromley & Ekdale, 1984). Thus, the presence of *Chondrites* is generally taken to infer dysoxic to anoxic pore waters, while monospecific suites of *Chondrites* record dysoxic bottom waters with even further reduced pore waters (e.g. Bromley & Ekdale, 1984; Savrda & Bottjer, 1987; Bromley, 1996; Savrda, 1998; Knaust, 2017). *Chondrites* commonly occurs at other Cenomanian–Turonian OAE2 localities within the WIS (Savrda, 1998; Sageman, 1989; Kauffman & Sageman, 1990; Grosskopf, 2015), and its abundance increases along the west-to-east deoxygenation gradient, particularly in more carbonate-rich southern intervals from Colorado to Kansas (e.g. Savrda, 1998). As such, it is surprising that *Chondrites* is absent from the OAE2-equivalent interval of this study, and the entirety of the encapsulating L2WS (representing peak transgression).

The general absence of *Chondrites* in this study is interpreted to reflect a combination of environmental stressors. These include salinity stress, particularly notable in the Belle Fourche (Facies 1), as *Chondrites* typically represents fully marine conditions (e.g. MacEachern *et al.*, 2007; Gingras *et al.*, 2011; Paz *et al.*, 2023); substrate instability, especially in intervals dominated by fluid muds that preclude stable, open burrow systems (e.g. Wetzel & Uchman, 1998); elevated nutrient availability, which reduces the necessity for specialised deep-tier deposit feeders at organic-rich levels (>2% TOC; Wetzel, 1983, 1991); and transient oxygenation, since sustained deep-tier feeding behaviours require stable, well-oxygenated conditions due to higher metabolic demands compared to shallow-tier mobile deposit feeding (Buatois *et al.*, 2011; Sperling *et al.*, 2013; Desai & Biswas, 2018). *Chondrites* within this core is rarely monospecific and most often present in intervals with the highest ichnodiversity. This association strongly suggests that at this location, *Chondrites* was most often emplaced during times of sustained bottom water oxygenation or dysoxia (e.g. relatively stable/equilibrium conditions). These relatively stable conditions allowed: (i) colonisation by various organisms with differing feeding strategies (in this core *Chondrites* is associated with the most ichnologically diverse intervals); and (ii) time for the construction of these complex permanent features. Thus, *Chondrites* herein may act as a visual proxy for sustained partially oxygenated bottom waters in Fig. 10.

Interpretations of ichnoguild distributions

Ichnoguild analysis provides a simple visual proxy for changing physicochemical stresses over the length of this core (e.g. the coloured ichnogenera columns in Fig. 10). Several physicochemical interpretations can be made by looking strictly at the ichnoguild distributions plotted on Fig. 10.

The prevalence of the fugichnia ichnoguild indicates the interval was prone to episodic sedimentation, while the specific distribution of navichnia indicates a waning river influence through time. The *Planolites* ichnoguild alone suggests the Belle Fourche Formation and middle and uppermost 2WS intervals possessed the most oxygenated pore waters, and when combined with the other ichnoguilds suggests pore-water oxygenation within the Lower 2WS dropped off rapidly and seemingly declined through time. Elements of the *Phycosiphon* ichnoguild fluctuate throughout this cored interval but generally increase in abundance upwards, indicating a gradual return to stable marine conditions (e.g. normal marine salinities and oxygenation). The inverse relationship between elements of the fugichnia and *Phycosiphon* ichnoguilds corroborates decreased deltaic influence over the depositional lifetime of this core. Similar to the *Planolites* ichnoguild, the distribution of the *Phycosiphon* ichnoguild indicates increasingly stable conditions after the termination of the Lower 2WS, with an apparent peak in stability in the uppermost 2WS. The distribution of the *Chondrites* ichnoguild indicates that the Belle Fourche Formation and middle and uppermost 2WS intervals were at least punctuated by periods of sustained bottom water oxygenation. Overall, ichnoguild analysis indicates that the Belle Fourche Formation and uppermost 2WS experienced the least oxygen stress.

DISCUSSION

Ichnological expressions of stress

The entire cored interval displays a common theme of diminutive and diminished ichnological suites. In general, the small body sizes and low diversity of infaunal traces are a clear response to imposed stresses acting at, or just below, the sediment–water interface. Sedimentological and ichnological features indicate three main physicochemical stressors acting throughout the deposition of this core, including: (i) reduced oxygenation; (ii) reduced salinity; and (iii) rapid/episodic sedimentation. These stressors are reflected in various proportions over time (e.g. facies and ichnoguild interpretations).

Reduced DO_2 in bottom waters and sediment pore waters is reflected as a marked decline in trace fossil size, ichnogenera diversity and depth of burrow penetration (e.g. Rhoads & Morse, 1971; Bromley & Ekdale, 1984; Savrda & Bottjer, 1987, 1989, 1991, 1994; Gingras *et al.*, 2011; MacEachern *et al.*, 2012; Dashtgard *et al.*, 2015; Dashtgard & MacEachern, 2016). Reductions in body size stem from a strategic adaptation to improve oxygen diffusion through an increased body surface area to volume ratio (Moore & Francis, 1985), ichnogenera diversity declines to accommodate only those species adapted to reduced oxygenation (e.g. modern-day nemerteans and nematodes) and depth of penetration is reduced due to a shallowing in the RPD within the sediments. Although this core displays all the characteristic signs of oxygen depletion, similar ichnological expressions could result from other stressors, or a complex combination of a variety of acting stressors.

The interpretation that many of the normally graded beds throughout this core represent rapid deposition of river-derived wave-supported hyperpycnites (e.g. Table 1) suggests an imposed reduction in salinity. Paralleling low-oxygen conditions, reduced salinity can lead to low-diversity suites of simplistic infaunal feeding behaviours (e.g. *Planolites*) and diminutive burrow sizes (e.g. Beynon *et al.*, 1988; Pemberton & Wightman, 1992; Gingras *et al.*, 1999, 2011, 2025; Bann *et al.*, 2004; Bann & Fielding, 2004; Buatois *et al.*, 2005, 2011; MacEachern *et al.*, 2007, 2012; MacEachern & Gingras, 2007; MacEachern & Bann, 2020). Reduced body size may be ascribed to a prevailing juvenile community, owing to shortened lifespans attributed to difficulties in ionic- and osmoregulation under salinity-reduced conditions (Gingras *et al.*, 2011; MacEachern *et al.*, 2012). Diminutive suites may also be a strategic adaptation to improve oxygen diffusion (or other solute transport) over an increased body surface area (Gingras *et al.*, 1999, 2011; MacEachern & Gingras, 2007), as reduced salinities impose an increased biologic oxygen requirement (Rees *et al.*, 1977; MacEachern *et al.*, 2012).

Although reductions in available DO_2 and salinity produce similar effects within an ichnological suite, they favour different trace fossil types. Low-oxygen settings show extremely impoverished ichnological suites dominated by diminutive infaunal deposit-feeding burrows typical of fully marine salinities (e.g. *Phycosiphon*, *Chondrites*) (e.g. Bromley & Ekdale, 1984; Ekdale & Mason, 1988; Wignall, 1991; Savrda, 1995, 2007; Gingras *et al.*, 2011), while reduced salinity settings show various simple diminutive deposit-feeding traces (e.g. *Planolites*, *Cylindrichnus*) (Howard & Frey, 1975; Gingras *et al.*, 1999, 2011, 2025; MacEachern & Gingras, 2007; Dashtgard *et al.*, 2008).

Intervals of rapid and episodic deposition (e.g. tempestites, hyperpycnites, wave-enhanced sediment gravity flows) are typified by low intensity, non-uniform (sporadic) and top-down ('lam-scram') reworking by transient simplistic feeding behaviours (e.g. those of *Planolites* and *Phycosiphon*), in combination with an abundance of rapid movement structures (e.g. fugichnia, navichnia) (Howard, 1975; Seilacher, 1982; Frey, 1990; Pemberton *et al.*, 1992; Leithold, 1993; Leithold & Dean, 1998;

MacEachern *et al.*, 2005, 2012; MacEachern & Bann, 2020). Sporadic top-down reworking and indistinct sediment mottling are owing to rapid sediment accumulation impeding the construction of permanent and semi-permanent domiciles, while associated clastic dilution leads to reduced nutrient density; both favouring transient feeding behaviours (MacEachern *et al.*, 2005, 2012). Additionally, rapid deposition results in sediments promptly passing through the RPD, imposing an oxygen stress, precluding endobenthic organisms and hindering even deep-tier deposit feeders (e.g. *Chondrites*) (MacEachern *et al.*, 2005, 2012; MacEachern & Bann, 2020).

Ichnological relative oxygen curves

Ichnological reconstruction of relative oxygen curves is not a novel concept (e.g. Savrda & Bottjer, 1986, 1991, 1994; Tyszka, 1994; Wan *et al.*, 2003; Rodríguez-Tovar *et al.*, 2009; Allington-Jones *et al.*, 2010). Rodríguez-Tovar *et al.* (2009) used ichnological diversity counts to generate an oxygen curve for the OAE2-bearing interval in pelagic and hemipelagic deposits near Manilva, Spain (fig. 4 in Rodrí guez-Tovar *et al.*, 2009). Changes in burrow diameter (i.e. size) were used to interpret oxygen fluctuations throughout the hemipelagic OAE2-bearing interval in Tibet (Wan *et al.*, 2003). The Size-Diversity Index (SDI), calculated as the product of ichnogenera diversity and maximum burrow diameter (*sensu* Hauck *et al.*, 2009), has been used as a proxy for both salinity (Hauck *et al.*, 2009; Gingras & MacEachern, 2012; Botterill *et al.*, 2015; Timmer *et al.*, 2016) and oxygenation stress (Furlong, 2019; González *et al.*, 2022). Herein, Fig. 10 illustrates three ways to reconstruct relative DO_2 levels: (i) diversity plots (purple column), (ii) maximum burrow diameters (green column), and (iii) the Size-Diversity Index (blue column). The diversity plots indicate the highest oxygen concentrations in the Upper 2WS. The maximum burrow diameters indicate the highest oxygen concentrations in the Belle Fourche and Upper 2WS Formations. The SDI curve combines and exaggerates the trends in the diversity and diameter curves, indicating that oxygenation was highest in the Upper 2WS. Further, each of the three potential proxy curves suggests that oxygenation was never stable, but rather constantly fluctuating, with the lowest oxygen conditions in the upper portion of the Lower 2WS.

Oxygen scenarios

The combined ichnological and sedimentological intricacies of this core suggest five prevailing oxygen scenarios: (i) moderately dysoxic bottom waters (OS1), (ii) severely dysoxic bottom waters (OS2), (iii) extremely dysoxic bottom waters (OS3), (iv) storm injection of oxygen under extremely dysoxic bottom waters (OS4) and anoxia (OS5) (using the oxygen terminology and saturation cut-offs outlined by Tyson & Pearson (1991)). Descriptions and interpretations of each scenario are summarised in Table 3.

Reflections of Oceanic Anoxic Event 2 (OAE2)

The carbon isotope curve for this core places the OAE2 between 2781 m and 2787.5 m depth (Figs 10 and 16), showing a rapid +2 $\delta^{13}C$ increase with the return to background values, or 'lapsing', apparently beginning at 2783.5 m.

Pre-OAE2

The Belle Fouche interval (Facies 1, deposited before transgression and the CIE) displays pronounced trace fossil diminution compared to typical salinity-stressed intervals (e.g. MacEachern & Bann, 2020), indicating an imposed deoxygenation stress before the onset of the OAE2. Deposits of the Belle Fourche Formation at this location are interpreted to reflect moderately dysoxic bottom waters (OS1).

A lithological change begins 3 m below the onset of the OAE2, gradually shifting from the interpreted most proximal coarsest-grained deposits (Facies 1) to well-established distal calcareous fine-grained deposits (Facies 5) of the L2WS <20 cm above the initial excursion (Figs 10 and 16). This is consistent with the regional deepening of the WIS noted from the southern (American) intervals (e.g. Arthur & Sageman, 2005). This lithological shift is concomitant with a dramatic pause in bioturbation, occurring roughly 30 cm (2787.80 m, Fig. 16) before the OAE2-bearing interval. The total preclusion of infauna is indicative of likely anoxia (OS5). Sedimentation rates calculated from Sageman *et al.*'s (2006) total CIE duration estimates in the WIS of 847 to 885 kyr place this initial temporary anoxic event 39 to 41 kyr in advance of the global definition (CIE) of OAE2 onset. Higher resolution carbon isotope analysis would undoubtedly help resolve this timeline. Other geochemical studies have noted excursions beginning shortly before the onset of the CIE.

Table 3. Descriptions and interpretations of the four oxygen scenarios.

Scenario		Description	Interpretation	DO_2 (mL/L)
OS1	Moderately dysoxic bottom waters	Diverse ichnological suites, and relatively large burrow diameters (max of 6 mm) Primary sedimentary features are only unreworked if the depositional bed is either thicker than the deepest extents of bioturbation (dictated by the RPD; e.g. thick tempestites, Fig. 11B); if sediment character is unfavourable to burrowing benthos (e.g. soup ground hyperpycnites, e.g. Fig. 11D)	Various physico-chemical stressors to account for diminutive trace sizes, including prevailing rapid sedimentation, periodically reduced salinities and bottom waters at <100% DO_2 saturation	<2.0
OS2	Severely dysoxic bottom waters	Low diversity suites, commonly monospecific *Planolites* and *Phycosiphon*. Common meiofaunal reworking Thick beds preserve remnant 'fuzzy' primary structures (Fig. 12C,D), while complete obliteration of primary sedimentary features occurs only in some thin beds. Typically bases of thin (<1 cm thick) episodic sedimentation events remain uncolonised	Shallow RPD in the sediments, associated with very low bottom water DO_2 diffusion	<1.0
OS3	Extremely dysoxic bottom waters	General preclusion of macroscopic trace fossils. Primary sedimentary features remain intact and show some 'fuzziness' (Fig. 12A,B)	Sustained extreme dysoxia with the RPD near or at the sediment–water interface	<0.5
OS4	Episodic oxygen injection under extremely dysoxic bottom waters	Macroscopic burrows (>1 mm) are confined to coarser grained storm beds but absent in fair weather or thin episodically emplaced deposits (e.g. IBF2 in the coarser-grained bed, while cryptic 'fuzzy' reworking characterises the thinner beds in Fig. 12C,D). Macroscopic burrows are overprinted by meiofaunal reworking (e.g. burrows become 'fuzzy') Mix of thin, generally unbioturbated beds intercalated with less common thicker and coarser bioturbated storm beds	Background conditions: Sustained extreme dysoxia with the RPD near or at the sediment–water interface Storm conditions: Mixing and water column turnover results in temporarily oxygenated bottom waters and pore waters of the incipient deposit. Macroscopic reworking may have occurred relatively quickly by transported adult organisms that had become entrained in the storm deposits (i.e. 'doomed pioneers'), or by rapid colonisation of larvae post-storm	<0.5 to <2.0
OS5	Anoxia	No biogenic reworking and all primary sedimentary structures intact with no 'fuzziness'	Anoxic bottom waters precluding epi- and infaunal life	0.0

Ostrander *et al.* (2017) noted a positive thallium excursion ~43 kyr before the onset of the CIE at the ODP Site 1258 (Demerara Rise, Atlantic), interpreted as bottom water deoxygenation prior to the OAE2. Turgeon & Creaser (2008) identified an osmium excursion occurring ~23 kyr before the onset of the OAE2 at both ODP site 1260B and Furlo Italy, indicating an extensive

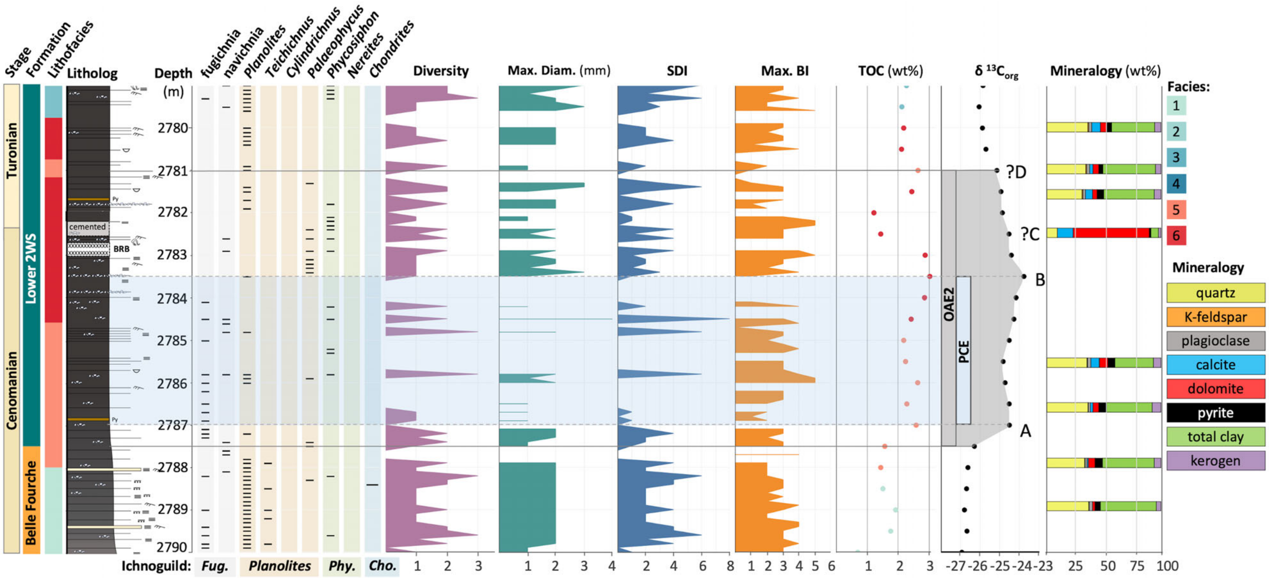

Fig. 16. Facies, ichnologic data, TOC (wt%), carbon isotopes and XRF-derived mineralogy (Percy & Pedersen, 2020) over the OAE2 interval. Ichnogenera organised by their ichnoguild association (coloured bars match colours in Table 2). The OAE2 interval outlined by the carbon isotope curve has been separated into 'A', 'B', 'C' and 'D' 'peaks' after O'Connor *et al.* (2020).

magmatic pulse and change to seawater chemistry. Montoya-Pino *et al.* (2010) and Clarkson *et al.* (2018) interpreted pre-CIE anoxia using uranium isotopes at Demerara Rise and European shelf/Tethyan margin, respectively. This pre-OAE2 deoxygenation is difficult to match to southern portions of the WIS, as US deposits largely reflect an initial trend towards better-oxygenated conditions at the onset of the OAE2 as the southern Texan sill was breached during transgression (e.g. Arthur & Sageman, 2005; Elderbak & Leckie, 2016; Lowery *et al.*, 2018), followed by a gradual return to more weakly oxygenated conditions throughout the duration of the event (Meyers *et al.*, 2005; Sageman *et al.*, 2024).

OAE2

Herein, the onset of the OAE2 CIE is near coeval with the Belle Fourche to L2WS transition. Lithologically the OAE2-bearing interval is characterised by the most distal and sediment-starved Facies 5 and 6. Mineralogically, the OAE2-bearing interval begins with an increase in total carbonate content (Figs 10 and 16), consistent with the mineralogical trends identified in the southern WIS (Arthur & Sageman, 2005). This increase in carbonate validates the idea that enrichment stems from increased production and/or decreased dilution accompanying water column deepening. Organic enrichment (TOC%) increases relatively dramatically (>1%) at the CIE, with maximums coinciding with the highest $\delta^{13}C$ values throughout the core. This increase in enrichment seemingly corroborates the incidence of most intense oxygen depletion for the entire cored interval (Demaison & Moore, 1980; Arthur and Sageman, 2005).

Ichnologically, the OAE2-bearing interval exhibits a reduction in trace fossil occurrence, accompanied by subtle decreases in trace fossil diversity, burrow sizes and bioturbation intensity (BI) (Figs 10 and 16). These ichnological attributes suggest elevated chemical stress compared to the underlying Facies 1 of the Belle Fourche Formation, where depositional conditions were primarily controlled by energy levels and intermittent salinity stress. This transition is interpreted to reflect a shift from moderately dysoxic bottom water conditions (OS1) in the Belle Fourche Formation towards fluctuating severe to extreme dysoxia (OS2 and OS3) within the OAE2-bearing interval.

The most notable characteristic over the CIE is the continued punctuation of the ichnological DO_2 proxy curves with relatively thick (>10 cm, up to 50 cm) intervals lacking biogenic evidence. These relatively thick depauperate intervals occur in the thin-bedded sediment-starved Facies 5 and thus are not the result of thick storm bed emplacement. Rather, the punctuating absence of infauna is attributed to intermittent anoxia (OS5) precluding the development of an infaunal community. This is most likely linked to an encroaching or developing oxygen minimum zone (OMZ) accompanying transgression and increased productivity. The spread in TOC values over the (interpreted above) sediment-starved OAE2-bearing interval is most likely the result of fluctuating primary productivity and variable organic degradation rates at the sea floor (i.e. the spread in values is not the product of variable dilution). These productivity fluctuations are likely climactically driven, where humid conditions lead to enhanced weathering and nutrient input causing increased primary production and oxygen consumption at the sea floor (e.g. Leckie *et al.*, 1998; Meyers *et al.*, 2001; Barclay *et al.*, 2010; Bryant *et al.*, 2021; Fortiz *et al.*, 2024), combined with lowered oxygen solubility in warmer waters. Bottom waters would have been anoxic only temporarily during peak productivity. Additionally, isolated bioturbated beds throughout the OAE2-bearing interval are interpreted as reflecting brief episodes of storm-driven oxygenation of the seafloor (OS4), rather than sudden, significant reductions in productivity.

Overall, the palaeo-oxygen interpretations herein suggest that the OAE2 was not a rapidly induced and temporally isolated event. Instead, it represents continuous oxygen fluctuations between periods of extreme deoxygenation punctuated by more oxygenated intervals. Intermittent deoxygenation has become the favoured interpretation over persistent anoxia for other globally diverse deposits that reflect oxygen stress over the OAE2, including the American extent of the WIS (Eicher & Diner, 1985; Sageman, 1989; Savrda & Bottjer, 1994; Sageman *et al.*, 1997; Savrda, 1998; Meyers *et al.*, 2001; Keller *et al.*, 2004; Meyers *et al.*, 2005; Bryant *et al.*, 2021; Bryant & Belanger, 2023; Sageman *et al.*, 2024), the northern Tethyan Margin (Switzerland, Westermann *et al.* (2010); Germany, Friedrich *et al.* (2011); Spain, Rodríguez-Tovar *et al.* (2009)), the southern Tethyan Margin (Tibet, Wan *et al.* (2003)) and the proto-Atlantic Ocean (Friedrich *et al.*, 2006).

The Plenus Cold Event

The extreme burial of organic carbon in marine sediments, reflected in the globally recorded CIE, may have forced atmospheric CO_2 drawdown, leading to subsequent climactic cooling and reinvigorated bottom water oxygenation shortly after the onset of OAE2 conditions (Schlanger & Jenkyns, 1976; Arthur *et al.*, 1987). Palaeontologic and geochemical analyses of globally diverse OAE2-bearing intervals confirm such an event, now recognised as the *Plenus Cold Event* (PCE) (e.g. Gale and Christensen, 1996; Wilmsen *et al.*, 2007; Forster *et al.*, 2007; Jarvis *et al.*, 2011; van Helmond *et al.*, 2016; Eldrett *et al.*, 2017; Clarkson *et al.*, 2018; Gale *et al.*, 2019; Boudinot and Sepúlveda, 2020; Percival *et al.*, 2020; Falzoni and Petrizzo, 2022).

The poor resolution carbon isotope curve and lack of detailed micropalaeontologic data herein make it difficult to place the PCE (the PCE corresponds with the foraminiferal 'Benthonic Zone' of Eicher & Worstell (1970); e.g. Elderbak & Leckie (2016)). Assigning diagnostic CIE 'peaks' after O'Connor *et al.* (2020), and crudely matching the overall shape of the carbon isotope curve to that of higher resolution data sets from the southern WIS (Pratt, 1984; Sageman *et al.*, 2006, 2024), places the PCE in the lower half of the CIE, spanning 2787.00 to 2785.50 m (Fig. 16, between peaks 'A' and 'B'). Despite the suggestion of a cold event from other localities, several studies from the southern WIS interpret the PCE-equivalent as representing a time of warming indicated by an influx of warm-water taxa (e.g. Corbett & Watkins, 2013; Elderbak and Leckie, 2016; Sageman *et al.*, 2024).

The detailed ichnological data set herein shows some differences between the interpreted PCE-equivalent and the upper portion of the OAE2-bearing interval (Fig. 16). Deposits incorporating the PCE display similar punctuations in biogenic reworking as the post-PCE OAE2-bearing interval (e.g. punctuation of BI data on Figs 10 and 16), but prolonged punctuations in other ichnological characteristics (diversity, diameter, SDI). This is attributed to much of the lower OAE2-bearing interval being bioturbated by exceptionally small trace-makers that could not be confidently attributed to specific ichnogenera (characteristic of OS3), and the more common occurrence of fugichnia and navichnia of which there is no causative burrow to take true diameter measurements. Alone, the occurrence of smaller burrows in the PCE-bearing interval suggests more oxygen-depleted bottom waters compared to deposits accumulating post-PCE (e.g. OS3 versus OS2, respectively). However, the more common occurrence of fugichnia and navichnia indicates a more energy- and salinity-stressed setting (see discussion in Section Ichnoguilds), which may also lead to diminutive infauna. Furthermore, it is important to note that deposits which accumulated post-PCE during the OAE2 interval are characterised entirely by Facies 6, reflecting a more sediment-starved setting than Facies 5, which characterises the PCE-bearing interval. This distorts the visual representation of the ichnological data on Fig. 16. Organic enrichment in the PCE and post-PCE intervals are similar (excluding the two low values taken near the Bighorn River Bentonite and the cemented CTB section). Considering sediment starvation (i.e. reduced dilution) in the post-PCE interval, conditions may reflect lower productivity and/or improved bottom water oxygenation compared to the more diluted PCE interval. However, available data do not allow a confident assessment of whether the PCE-equivalent was more or less oxygenated than the post-PCE. Overall, the entire OAE2-bearing interval experienced significant deoxygenation (severely to extremely dysoxic; OS2–3), with only intermittent episodes of anoxia (OS5).

Post-OAE2

The return of the CIE to background levels at the base of the L2WS marks the end of OAE2 (Figs 10 and 16). Ichnological data indicate persistently low bottom water oxygenation post-OAE2, fluctuating between severely and extremely dysoxic (OS2–3), with infrequent and less intense anoxic episodes (OS5), as shown by thinner and infrequent burrowed levels. Oxygen fluctuations and intermittent anoxia persisted through most of the L2WS, supported by continued variability in organic enrichment. This pattern agrees with southern WIS interpretations of ongoing production-driven deoxygenation (e.g. Meyers *et al.*, 2005; Bryant *et al.*, 2021).

In the M2WS, bottom water conditions improve, evidenced by fewer ichnological interruptions and a modest increase in bioturbation intensity (Fig. 10). More consistent biogenic reworking suggests stable oxygen conditions, and increased diversity relative to the pre-OAE2 interval indicates reduced salinity stress (Facies 2 versus Facies 1). Burrow sizes remain comparable to those in the Belle Fourche Formation, suggesting lingering oxygen stress.

The U2WS begins with a sharp rise in bioturbation (obscuring diversity and size measurements), followed by ichnological metrics similar to the pre-OAE2 Belle Fourche interval—indicating improved oxygenation relative to the L2WS. Its upper portion shows a marked increase across all DO_2 proxy data, signalling the most hospitable bottom water conditions since the onset of L2WS deposition.

Interval of most intense deoxygenation

The carbon isotopes, lithology, TOC values, mineralogy and ichnological trends may lead one to assume that the isotopically defined OAE2 reflects the lowest oxygenation experienced over the depositional lifetime of this core. Again, the ichnological DO_2 proxy curves (e.g. diversity, diameter, SDI; Figs 10 and 16) corroborate intermittent deoxygenation. However, it is not until approximately 14 m above the termination of the OAE2, within the uppermost portion of the L2WS, that the ichnology reflects the lowest relative oxygen concentrations (Fig. 11). This interval lithologically, geochemically (TOC%), and mineralogically mirrors that of much of the basal L2WS and the encapsulated OAE2. Here, the ichnology marks this interval as having suffered the most intense oxygen depletion. The more frequent punctuations in all biogenic data, including BI, indicate more frequent anoxia than occurred during the OAE2. More frequent dysoxia is indicated by the common occurrence of bioturbated intervals lacking distinct burrow data (diversity and size), attributed to biogenic reworking exclusively by meiofauna or exceedingly small macrofauna.

This temporal disconnect between the isotopically defined OAE2, and the peak deoxygenation higher up, has been geochemically and palaeontologically identified in the southern portion of the WIS (Savrda, 1998; Meyers *et al.*, 2001, 2005; Meyers & Sageman, 2007; Dale *et al.*, 2012; Elderbak & Leckie, 2016). The consensus is that this is likely a factor of continued (peak) transgression and development of an oxygen minimum zone, peaking in the early Turonian after cessation of the OAE2 CIE (Meyers *et al.*, 2005; Elderbak & Leckie, 2016; Bryant *et al.*, 2021).

Both Facies 5 (pin-striped) and 6 (silt-streaked), which characterise the OAE2-bearing deposits (Figs 8 to 10), reflect storm wave reworking leading to the winnowing and accumulation of the larger grains into stripes and streaks (Table 1). This rather continuous, albeit relatively low-energy sea floor wave action would provide some oxygen invigoration to the bottom waters, precluding the development of sustained anoxia (e.g. Stel, 1975;

Macquaker, 1987; Savrda & Bottjer, 1991; Schieber, 1994; Wignall & Myers, 1988; Allington-Jones *et al.*, 2010; Comerio *et al.*, 2018; Algeo & Li, 2020). This reworking is further interpreted to be the exact mechanism leading to the peak in organic enrichment in the OAE2-bearing interval (Percy & Pedersen, 2020). This interval reflects the coarsest grain sizes (in terms of *functional* depositional grain size) throughout the entire core (e.g. fig. 2 in Percy & Pedersen, 2020), as mud constituents were deposited as intraclastic aggregates (i.e. previously deposited, eroded and re-transported composite particles of mud, organic matter and other detritus). The sheltering of organic matter in transported composite particles prevents any further degradation (e.g. Biddle *et al.*, 2025). The higher up interval reflecting peak deoxygenation is characterised solely by the distal and low-energy silt-streaked Facies 6, and the mud constituents are not functionally as coarse-grained (identified to be smaller aggregates by Percy & Pedersen, 2020). These smaller aggregates provide lesser organic matter sheltering, and thus the relatively high TOC values are likely the result of heightened productivity over increased preservation potential. The deeper water column here (associated with peak transgression) compared to the OAE2-bearing interval prevented storm-generated bottom water oxygen invigoration. This allowed the poorly sheltered organic matter to frequently exhaust the limited oxygen supply during degradation.

Corroborating peak deoxygenation tied to peak transgression is the delayed northward migration of the thermal front between the cold and better-oxygenated northern-sourced Boreal waters and the warm, less oxygenated southern-sourced Tethyan incursion. The density contrast between these two water masses resulted in their segregation. Slingerland *et al.* (1996) proposed a model for Early Turonian WIS circulation with counterclockwise flow: Boreal waters migrated south along the western margin, while Tethyan waters moved north along the eastern margin, driven partly by shore-parallel freshwater currents (e.g. fig. 7 in Arthur & Sageman, 2005). This circulation ultimately produced a north–south directed front at the northern extent and a remnant east–west front to the south (Eicher & Diner, 1985; Leckie *et al.*, 1998; Savrda, 1998; Slingerland *et al.*, 1998; Fisher & Arthur, 2002; Fisher, 2003; Denne *et al.*, 2014; Lowery *et al.*, 2018; Sageman *et al.*, 2024). The northward migration of less oxygenated waters was tracked by Bryant & Belanger (2023), where more northern locations in the American portion of the WIS experienced less severe and delayed oxygen depletion over the CTB when compared to the south. In their study, the lowest oxygen levels occurred above the OAE2 CIE, similar to the pattern observed in this study.

CONCLUSIONS AND SUMMARY

In-depth ichnological analyses revealed more diverse and more frequent bioturbation than previously documented for the 2WS interval. The generally diminutive and diminished ichnological suite herein indicates a perpetually physiochemically stressed setting. Integration of trace fossil characteristics with sedimentology indicates a variety of stressors, including oxygen, salinity, energy and episodic sedimentation in varying proportions. Four distinct ichnoguilds were constructed by grouping ethologically similar ichnogenera. Plotting ichnoguild distributions over the cored interval illuminated how physicochemical stresses, mainly oxygen, salinity and episodic sedimentation fluctuated through time.

Applying multiple ichnological analytical techniques (trace fossil characteristics, ichnofacies analysis, ichnoguild analysis and petrographic ichnology) allowed interpretation of five different bottom water oxygen scenarios for this setting, including (i) poorly oxygenated bottom waters, (ii) severely dysoxic bottom waters, (iii) extremely dysoxic bottom waters, (iv) episodic oxygen injection by storms and (v) anoxia.

Ichnologically interpreted low and constantly fluctuating bottom water oxygenation characterised the Cenomanian–Turonian boundary interval deposits containing OAE2 in west-central Alberta. During the OAE2 itself, bottom water oxygenation fluctuated between severely dysoxic (OS2), extremely dysoxic (OS3), temporarily oxygenated through storm injection (OS4) and intermittent anoxia (OS5). No confident distinction in oxygenation trends could be deduced between the PCE and the post-PCE within the OAE2, with both intervals displaying significant and fluctuating deoxygenation.

The entire OAE2-bearing interval (including the basal PCE interval) clearly displays depressed depositional oxygenation, but not the lowest documented for this core. Traditionally, peak deoxygenation for this core may have been associated with the highest TOC and $\delta^{13}C_{org}$ values (e.g. at approximately 2785 m) just below the CTB. However, the ichnological DO_2 proxy curves suggest instead that peak deoxygenation was reached roughly 20 m higher, in the middle of the Lower 2WS (e.g. 2763 m) and roughly 14 m after the termination of the OAE2. Peak deoxygenation in the younger interval is interpreted as a result of a deep-water column (peak transgression) and increased productivity, leading to limited water column turnover and increased oxygen consumption at the sea floor. Delayed Tethyan influence compared to southern WIS locations may further explain the lag in peak productivity.

A future high-resolution study combining these ichnological results with geochemical palaeoredox proxies (e.g. enrichment factors of molybdenum and vanadium) would help resolve the OAE2 boundaries and internal shifts (e.g. 'A', 'B' and 'C' of O'Connor *et al*. (2020)) in this area. This would be best accomplished by matching the ichnological and geochemical resolution over the same 10 cm intervals ('bins'). This integrated approach would further help refine and validate the oxygen trends proposed in this study.

ACKNOWLEDGEMENTS

Both authors acknowledge the support of the Natural Sciences and Engineering Research Council of Canada (NSERC), (MKG Discovery Grant RGPIN-2020-0513; SKB Postgraduate Scholarship [NSERC PGS-D]). Thank you to Per Pedersen at the University of Calgary for allowing us to sample the herein-studied drill core, and for providing invaluable discussions on the North American OAE2-encapsulating interval. Thank you to Steve Grasby at the Geological Society of Canada for funding the high-resolution carbon isotope and total organic carbon analysis. A further thank you to Chief Editors Gabriela Mángano and Marc Aurell Associate Editors Chris Fielding and John Reijmer, and reviewers Brad Sageman and two anonymous reviewers whose comments greatly improved this manuscript.

DATA AVAILABILITY STATEMENT

The data that support the findings of this study are available from the corresponding author upon reasonable request.

REFERENCES

Alberta Geological Survey. (2015) Alberta table of formations, Alberta energy regulator. Available at: http://ags.aer.ca/document/Table-of-Formations.pdf.

Algeo, T.J. and **Li, C.** (2020) Redox classification and calibration of redox thresholds in sedimentary systems. *Geochim. Cosmochim. Acta*, **287**, 8–26.

Allington-Jones, L., **Braddy, S.J.** and **Trueman, C.N.** (2010) Palaeoenvironmental implications of the ichnology and geochemistry of the Westbury Formation (Rhaetian), Westbury-on-Severn, south-west England. *Palaeontology*, **53**, 491–506.

Arthur, M.A. and **Sageman, B.B.** (2005) Sea-level control on source-rock development: perspectives from the Holocene Black Sea, the mid-Cretaceous Western Interior Basin, and the late Devonian Appalachian basin. In: *The Deposition of Organic-Carbon-Rich Sediments: Models, Mechanisms, and Consequences* (Ed. Harris, N.B.), *SEPM Spec. Publ.*, **82**, 35–59. Tulsa, OK.

Arthur, M.A. and **Schlanger, S.O.** (1979) Cretaceous "oceanic anoxic events" as causal factors in development of reef- reservoired giant oil fields. *AAPG Bull.*, **63**, 870–885.

Arthur, M.A., **Schlanger, S.O.** and **Jenkyns, H.C.** (1987) The Cenomanian-Turonian Oceanic Anoxic Event, II. Palaeoceanographic controls on organic-matter production and preservation. *Geol. Soc. Lond. Spec. Publ.*, **26**, 401–420.

Bann, K.L. and **Fielding, C.R.** (2004) An integrated ichnological and sedimentological comparison of non-deltaic shoreface and subaqueous delta deposits in Permian reservoir units of Australia. *Geol. Soc. Lond. Spec. Publ.*, **228**, 273–310.

Bann, K., **Fielding, C.R.**, **MacEachern, J.A.** and **Tye, S.** (2004) Distinction between offshore marine and fine-grained coastal facies using integrated ichnology and sedimentology: the Permian Pebbley Beach Formation, southern Sydney Basin, Australia. In: *The Application of Ichnology to Palaeoenvironmental and Stratigraphic Analysis* (Ed. D. McIlroy), *Geol. Soc. Lond. Spec. Pub.*, **228**, 179–212.

Barclay, R.S., **McElwain, J.C.** and **Sageman, B.B.** (2010) Carbon sequestration activated by a volcanic CO_2 pulse during Ocean Anoxic Event 2. *Nat. Geosci.*, **3**, 205–208.

Barker, I.R., **Moser, D.E.**, **Kamo, S.L.** and **Plint, A.G.** (2011) High-precision U–Pb zircon ID–TIMS dating of two regionally extensive bentonites: Cenomanian Stage, Western Canada Foreland Basin. *Can. J. Earth Sci.*, **48**, 543–556.

Beaumont, C. (1981) Foreland basins. *Geophys. J. R. Astron. Soc.*, **65**, 291–329.

Bednarz, M. and **McIlroy, D.** (2009) Three-dimensional reconstruction of "phycosiphoniform" burrows: implications for identification of trace fossils in core. *Palaeontol. Electron.*, **12**, 1–15.

Beynon, B.M., **Pemberton, S.G.**, **Bell, D.A.** and **Logan, C.A.** (1988) Environmental implications of ichnofossils from the Lower Cretaceous Grand Rapids Formation, Cold Lake Oil Sands Deposit. In: *Sequences, Stratigraphy, Sedimentology: Surface and Subsurface* (Eds James, D.P. and Leckie, D.A.), *Soc. Petrol. Geol. Memoir*, **15**, 275–290.

Biddle, S.K., **LaGrange, M.T.**, **Harris, B.S.**, **Egenhoff, S.E.** and **Gingras, M.K.** (2025) Current concepts in mudstone description and deposition: a synthesis for mudstone initiates. *Sedimentologika*, **3**, 1–36. https://doi.org/10.57035/journals/sdk.2025.e31.1621.

Blakey, R.C. (2014) Paleogeography and paleotectonics of the western interior seaway, Jurassic-Cretaceous of North America. *Search Discov.*, **72**, 30392.

Bloch, J., **Schroder-Adams, C.**, **Leckie, D.A.**, **McIntyre, J.C.** and **Staniland, M.** (1993) Revised stratigraphy of the lower Colorado Group (Albian to Turonian), western Canada. *Bull. Can. Petrol. Geol.*, **41**, 325–348.

Botterill, S.E., **Campbell, S.G.**, **Pemberton, S.G.** and **Gingras, M.K.** (2015) Process ichnological analysis of the Lower Cretaceous Bluesky Formation, Alberta. *Bull. Can. Petrol. Geol.*, **63**, 123–142.

Boucher, R.J. (2016) Mapping sweetness of the Second White Speckled Shale S Member: Ricinus Area, Alberta, Canada. Master of Science, University of Louisiana at Lafayette, University of Louisiana at Lafayette ProQuest Dissertations & Theses.

Boudinot, F.G. and **Sepúlveda, J.** (2020) Marine organic carbon burial increased forest fire frequency during Oceanic Anoxic Event 2. *Nat. Geosci.*, **13**(10), 693–698.

Bromley, R.G. (1996) *Trace Fossils: Biology, Taphonomy and Applications*, 2nd edn, p. 361. Chapman and Hall, London.

Bromley, R.G. and **Ekdale, A.A.** (1984) *Chondrites*: a trace fossil indicator of anoxia in sediments. *Science*, **224**, 872–874.

Bryant, R. and **Belanger, C.L.** (2023) Spatial heterogeneity in benthic foraminiferal assemblages tracks regional impacts of paleoenvironmental change across Cretaceous OAE2. *Paleobiology*, **49**, 431–453.

Bryant, R., **Leckie, R.M.**, **Bralower, T.J.**, **Jones, M.M.** and **Sageman, B.B.** (2021) Microfossil and geochemical records reveal high-productivity paleoenvironments in the Cretaceous Western Interior Seaway during Oceanic Anoxic Event 2. *Palaeogeogr. Palaeoclimatol. Palaeoecol.*, **584**, 110679.

Buatois, L.A. and **Mangano, M.G.** (2003) Early colonization of the deep sea: ichnologic evidence of deep-marine benthic ecology from the Early Cambrian of Northwest Argentina. *Palaios*, **18**, 572–581.

Buatois, L.A., **Gingras, M.K.**, **MacEachern, J.**, **Mangano, M.G.**, **Zonneveld, J.**, **Pemberton, S.G.**, **Netto, R.G.** and **Martin, A.** (2005) Colonization of brackish-water systems through time: evidence from the trace-fossil record. *Palaios*, **20**, 321–347.

Buatois, L.A., **Saccavno, L.L.** and **Zavala, C.** (2011) Ichnologic signatures of hyperpycnal flow deposits in Cretaceous river-dominated deltas, Austral Basin, Southern Argentina. In: *Sediment Transfer from Self to Deep Water – Revisiting the Delivery System* (Eds. Slatt, R.M. and Zavala, C.), *AAPG Stud. Geol.* 61, 153–170.

Clarkson, M.O., **Stirling, C.H.**, **Jenkyns, H.C.**, **Dickson, A.J.**, **Porcelli, D.**, **Moy, C.M.**, **Pogge von Stranmann, P.A.E.**, **Cooke, I.R.** and **Lenton, T.M.** (2018) Uranium isotope evidence for two episodes of deoxygenation during Oceanic Anoxic Event 2. *Proc. Natl Acad. Sci. USA*, **115**, 2918–2923.

Comerio, M., **Fernández, D.E.** and **Pazos, P.J.** (2018) Sedimentological and ichnological characterization of muddy storm related deposits: the upper Hauterivian ramp of the Agrio Formation in the Neuquén Basin, Argentina. *Cretac. Res.*, **85**, 78–94.

Corbett, M.J. and **Watkins, D.K.** (2013) Calcareous nannofossil paleoecology of the mid-Cretaceous Western Interior Seaway and evidence of oligotrophic surface waters during OAE2. *Palaeogeogr. Palaeoclimatol. Palaeoecol.*, **392**, 510–523.

Dale, A.W., **Meyers, S.R.**, **Aguilera, D.R.**, **Arndt, S.** and **Wallmann, K.** (2012) Controls on organic carbon and molybdenum accumulation in Cretaceous marine sediments from the Cenomanian-Turonian interval including Oceanic Anoxic Event 2. *Chem. Geol.*, **324**, 28–45.

Dashtgard, S.E. and **MacEachern, J.A.** (2016) Unburrowed mudstones may record only slightly lowered oxygen conditions in warm, shallow basins. *Geology*, **44**, 371–374.

Dashtgard, S.E., **Gingras, M.K.** and **Pemberton, S.G.** (2008) Grain-size controls on the occurrence of bioturbation. *Palaeogeogr. Palaeoclimatol. Palaeoecol.*, **257**, 224–243.

Dashtgard, S.E., **Snedden, J.W.** and **MacEachern, J.A.** (2015) Unbioturbated sediments on a muddy shelf: hypoxia or simply reduced oxygen saturation? *Palaeogeogr. Palaeoclimatol. Palaeoecol.*, **425**, 128–138.

Demaison, G.J. and **Moore, G.T.** (1980) Anoxic environments and oil source bed genesis. *Org. Geochem.*, **2**, 9–31.

Denne, R.A., **Hinote, R.E.**, **Breyer, J.A.**, **Kosanke, T.H.**, **Lees, J.A.**, **Engelhardt-Moore, N.**, **Spaw, J.M.** and **Tur, N.** (2014) The Cenomanian–Turonian Eagle Ford Group of South Texas: insights on timing and paleoceanographic conditions from geochemistry and micropaleontologic analyses. *Palaeogeogr. Palaeoclimatol. Palaeoecol.*, **413**, 2–28.

Desai, B.G. and **Biswas, S.K.** (2018) Postrift deltaic sedimentation in western Kachchh Basin: insights from ichnology and sedimentology. *Palaeogeogr. Palaeoclimatol. Palaeoecol.*, **504**, 104–124.

Dummann, W., **Wennrich, V.**, **Schröder-Adams, C.J.**, **Leicher, N.** and **Herrle, J.O.** (2024) Ash deposits link Oceanic Anoxic Event 2 to High Arctic volcanism. *Geology*, **52**, 927–932.

Eicher, D.L. and **Diner, R.** (1985) Foraminifera as indicators of water mass in the Cretaceous Greenhorn Sea, Western Interior. In: *Fine-grained deposits and biofacies of the Cretaceous Western Interior Seaway: evidence of cyclic sedimentary processes* (Eds. Prett, L.M., Kauffman, E.G. and Zelt, F.B.), *SEPM Field Trip Guide*, **4**, 60–71. Tulsa, Okla.

Eicher, D.L. and **Worstell, P.** (1970) Cenomanian and Turonian foraminifera from the great plains, United States. *Micropaleontology*, **16**, 269–324.

Ekdale, A.A. and **Mason, T.R.** (1988) Characteristic trace fossils associations in oxygen-poor sedimentary environments. *Geology*, **16**, 720–723.

Elderbak, K. and **Leckie, R.M.** (2016) Paleocirculation and foraminiferal assemblages of the Cenomanian–Turonian Bridge Creek Limestone bedding couplets: productivity vs. dilution during OAE2. *Cretac. Res.*, **60**, 52–77.

Elderbak, K., **Leckie, R.M.** and **Tibert, N.E.** (2014) Paleoenvironmental and paleoceanographic changes across the Cenomanian–Turonian Boundary Event (Oceanic Anoxic Event 2) as indicated by foraminiferal assemblages from the eastern margin of the Cretaceous Western Interior Sea. *Palaeogeogr. Palaeoclimatol. Palaeoecol.*, **413**, 29–48.

Eldrett, J.S., **Dodsworth, P.**, **Bergman, S.C.**, **Wright, M.** and **Minisini, D.** (2017) Water-mass evolution in the Cretaceous Western Interior Seaway of North America and equatorial Atlantic. *Clim. Past.*, **13**(7), 855–878.

Falzoni, F. and **Petrizzo, M.R.** (2022) Evidence for changes in sea-surface circulation patterns and ~20° equatorward expansion of the Boreal bioprovince during a cold snap of Oceanic Anoxic Event 2 (Late Cretaceous). *Glob. Planet. Chang.*, **208**, 103678.

Fisher, C. (2003) Planktic foraminiferal porosity: a water mass proxy for Latest Cenomanian Paleoceanography, Greenhorn Sea, Western Interior USA and Canada. *Cretac. Res.*, **24**, 633–651.

Fisher, C.G. and **Arthur, M.A.** (2002) Water mass characteristics in the Cenomanian US Western Interior seaway as indicated by stable isotopes of calcareous organisms. *Palaeogeogr. Palaeoclimatol. Palaeoecol.*, **188**, 189–213.

Forster, A., **Schouten, S.**, **Moriya, K.**, **Wilson, P.A.** and **Sinninghe Damsté, J.S.** (2007) Tropical warming and intermittent cooling during the Cenomanian/Turonian oceanic anoxic event 2: Sea surface temperature records from the equatorial Atlantic. *Paleoceanography*, **22**(1). https://doi.org/10.1029/2006pa001349.

Fortiz, V., **Oakes, R.**, **Boudinot, F.G.**, **Jones, M.M.**, **Leckie, R.M.**, **Parker, A.**, **Sageman, B.B.**, **Sepúlveda, J.** and **Bralower, T.J.** (2024) Paleoceanographic Significance of calcareous nannofossil assemblages in the Tropic Shale of Utah during Oceanic Anoxic Event 2 at the Cenomanian/Turonian Boundary. *Micropaleontology*, **70**, 205–224.

French, K.L., **Flaum, J.A.** and **Birdwell, J.E.** (2024) An integrated perspective of paleoenvironmental change in the Western Interior Seaway before and during OAE-2 reveals how organic-rich mudstones form in dynamic environments. *Earth Planet. Sci. Lett.*, **642**, 118850.

Frey, R.W. (1990) Trace fossils and hummocky cross-stratification, Upper Cretaceous of Utah. *Palaios*, **5**, 203–218.

Friedrich, O., **Erbacher, J.** and **Mutterlose, J.** (2006) Paleoenvironmental changes across the Cenomanian/Turonian boundary event (oceanic anoxic event 2) as indicated by benthic foraminifera from the Demerara Rise (ODP Leg 207). *Rev. Micropaléontol.*, **49**, 121–139.

Friedrich, O., **Voigt, S.**, **Kuhnt, T.** and **Koch, M.C.** (2011) Repeated bottom-water oxygenation during OAE 2: timing and duration of short-lived benthic foraminiferal repopulation events (Wunstorf, northern Germany). *J. Micropalaeontol.*, **30**, 119–128.

Furlong, C.M. (2019) High-resolution analysis of the ichnological diversity, depositional dynamics, and stratigraphic architecture of the Middle Triassic Sunset Prairie Formation. Doctoral Thesis, University of Alberta, ERA Citation and Research Archive. Available at: https://era.library.ualberta.ca/items/3f4c1ad4-0c7e-4d7f-8620-a4f6a997cdc4.

Furmann, A., **Mastalerz, M.**, **Schimmelmann, A.**, **Pedersen, P.K.** and **Bish, D.** (2014) Relationships between porosity, organic matter, and mineral matter in mature organic-rich marine mudstones of the Belle Fourche and Second White Specks formations in Alberta, Canada. *Mar. Pet. Geol.*, **54**, 65–81.

Furmann, A., **Mastalerz, M.**, **Brassell, S.C.**, **Pedersen, P.K.**, **Zajac, N.A.** and **Schimmelmann, A.** (2015) Organic matter geochemistry and petrography of Late Cretaceous (Cenomanian-Turonian) organic-rich shales from the Belle Fourche and Second White Specks Formations, west-central Alberta, Canada. *Org. Geochem.*, **85**, 102–120.

Furmann, A., **Mastalerz, M.**, **Bish, D.**, **Schimmelmann, A.** and **Pedersen, P.K.** (2016) Porosity and pore size distribution in mudrocks from the Belle Fourche and Second White Specks Formations in Alberta, Canada. *AAPG Bull.*, **100**, 1265–1288.

Gale, A.S. and **Christensen, W.K.** (1996) Occurrence of the belemnite Actinocamax plenus in the Cenomanian of SE France and its significance. *Bull. Geol. Soc. Den.*, **43**(1), 68–77.

Gale, A.S., **Jenkyns, H.C.**, **Tsikos, H.**, **Sinninghe Damst, J.S.**, **Bottini, C.**, **Erba, E.**, **Russo, F.**, **Petrizzo, M.R.**, **Dickson, A.J.** and **Wray, D.S.** (2019) High-resolution bio- and chemostratigraphy of an expanded record of Oceanic Anoxic Event 2 (late Cenomanian–early Turonian) at Clot Chevalier, near Barr.me, SE France (Vocontian Basin). *Newsl. Stratigr.*, **52**(1), 97–129.

Gingras, M.K. and **MacEachern, J.A.** (2012) Tidal ichnology of shallow-water clastic settings. In: *Principles of Tidal Sedimentology* (Eds Davies, R.A. and Dalrymple, R.W.), pp. 57–77. Springer New York, New York, NY.

Gingras, M.K., **Pemberton, S.G.**, **Saunders, T.** and **Clifton, H.E.** (1999) The ichnology of modern and Pleistocene brackish-water deposits at Willapa Bay, Washington: variability in estuarine settings. *Palaios*, **14**, 352.

Gingras, M.K., **Bann, K.L.**, **MacEachern, J.A.**, **Waldron, J.** and **Pemberton, S.G.** (2007) A conceptual framework for the application of trace fossils. In: *Applied Ichnology* (Eds. MacEachern, J.A., Bann, K.L., Gingras, M.K. and Pemberton, S.G.), *SEPM Short Course Notes*, **52**, 1–25. Tulsa.

Gingras, M.K., **MacEachern, J.A.** and **Dashtgard, S.E.** (2011) Process ichnology and the elucidation of physico-chemical stress. *Sed. Geol.*, **237**, 115–134.

Gingras, M.K., **MacEachern, J.A.**, **Dashtgard, S.E.** and **Bann, K.L.** (2025) The *Teichichnus* ichnofacies: its neoichnological basis and identification in the rock record. *Sedimentology*, **72**, 408–441.

Goldring, R., **Pollard, J.E.** and **Taylor, A.M.** (1991) *Anconichnus horizontalis*: a pervasive ichnofabric-forming trace fossil in post-Paleozoic offshore siliciclastic facies. *Palaios*, **6**, 250–263.

González, P.D., **Furlong, C.M.**, **Gingras, M.K.**, **Playter, T.** and **Zonneveld, J.-P.** (2022) Depositional framework and trace fossil assemblages of the Lower Triassic Montney Formation, northeastern British Columbia, Western Canada Sedimentary Basin. *Mar. Pet. Geol.*, **143**, 105822.

Goodarzi, F., **Hosseininejad, S.**, **Pedersen, P.K.**, **Gentzis, T.** and **Sanei, H.** (2022) Characterization of immature oil shales from the Cretaceous Second White Specks Formation in Saskatchewan and Manitoba, Canada. *Mar. Petrol. Geol.*, **143**, 105774.

Grosskopf, J.F. (2015) Using trace fossils to determine the role of Oceanic Anoxic Event II on the Cretaceous Western Interior Seaway paleoenvironment [Doctoral dissertation, Louisiana State University and Agricultural & Mechanical College].

Hancock, J.M. and **Kauffman, E.G.** (1979) The great transgressions of the Late Cretaceous. *J. Geol. Soc. Lond.*, **136**, 175–186.

Haq, B.U. (2014) Cretaceous eustasy revisited. *Glob. Planet. Chang.*, **113**, 44–58.

Hart, B.S., **Schieber, J.**, **Hofmann, M.H.** and **Plint, A.G.** (2024) Failure to launch: fate of the Second White Specks as a resource play was preordained by its Late Cretaceous depositional setting. *AAPG Bull.*, **108**(9), 1827–1848.

Hauck, T.E., **Dashtgard, S.E.**, **Pemberton, S.G.** and **Gingras, M.K.** (2009) Brackish-water ichnological trends in a microtidal barrier Island-embayment system, Kouchibouguac National Park, New Brunswick, Canada. *Palaios*, **24**, 478–496.

van Helmond, N.A., **Sluijs, A.**, **Papadomanolaki, N.M.**, **Plint, A.G.**, **Gröcke, D.R.**, **Pearce, M.A.**, **Eldrett, J.S.**, **Trabucho-Alexandre, J.**, **Walaszczyk, I.**, **van de Schootbrugge, B.** and **Brinkhuis, H.** (2016) Equatorward phytoplankton migration during a cold spell within the Late Cretaceous super-greenhouse. *Biogeosciences*, **13**, 2859–2872.

Hosseininejad Mohebati, S. (2016) Organic, Inorganic Geochemistry and Sedimentology of the Second White Specks Formation, Eastern Margin of the Western Interior Seaway. Doctoral Thesis, University of Calgary, Alberta, Canada.

Howard, J.D. (1975) The sedimentological significance of trace fossils. In: *The Study of Trace Fossils* (Ed Frey, R.W.), pp. 131–146. Springer, Berlin, Heidelberg.

Howard, J.D. and **Frey, R.W.** (1973) Characteristic physical and biogenic sedimentary structures in Georgia estuaries. *AAPG Bull.*, **57**, 1169–1184.

Howard, J.D. and **Frey, R.W.** (1975) Estuaries of the Georgia coast, U.S.A.: Sedimentology and Biology, II Regional animal-sediment characteristics of Georgia estuaries. *Senckenb. Marit.*, **7**, 30–103.

Howard, J.D., **Elder, C.A.** and **Heinbokel, J.F.** (1975) Animal-sediment relationships in estuarine point-bar deposits, Ogeechee River, Ossabaw Sound, Georgia. *Senckenb. Marit.*, **7**, 181–203.

Jarvis, I., **Lignum, J.S.**, **Gröcke, D.R.**, **Jenkyns, H.C.** and **Pearce, M.A.** (2011) Black shale deposition, atmospheric CO_2 drawdown, and cooling during the Cenomanian-Turonian Oceanic Anoxic Event. *Paleoceanography*, **26**(3). https://doi.org/10.1029/2010pa002081.

Jenkyns, H.C. (1980) Cretaceous anoxic events: from continents to oceans. *J. Geol. Soc. Lond.*, **137**, 171–188.

Jenkyns, H.C. (2010) Geochemistry of oceanic anoxic events. *Geochem. Geophys. Geosyst.*, **11**, Q03004.

Jenkyns, H.C. (2018) Transient cooling episodes during Cretaceous Oceanic Anoxic Events with special reference to OAE 1a (Early Aptian). *Phil. Trans. Roy. Soc. A*, **376**, 20170073.

Jones, M.M., **Sageman, B.B.**, **Selby, D.**, **Jicha, B.R.**, **Singer, B.S.** and **Titus, A.L.** (2021) Regional chronostratigraphic synthesis of the Cenomanian-Turonian Oceanic Anoxic Event 2 (OAE2) interval, Western Interior Basin (USA): new Re-Os chemostratigraphy and 40Ar/39Ar geochronology. *GSA Bull.*, **133**(5–6), 1090–1104.

Kauffman, E.G. (1977) Geological and biological overview: Western Interior Cretaceous basin. *Mt. Geol.*, **14**, 75–99.

Kauffman, E.G. (1984) Paleobiogeography and evolutionary response dynamic in the Cretaceous Western Interior Seaway of North America. *Geol. Assoc. Can. Spec. Pap.*, **27**, 273–306.

Kauffman, E.G. and **Caldwell, W.G.E.** (1993) The Western Interior Basin in space and time. *Geol. Assoc. Can. Spec. Pap.*, **39**, 1–30.

Kauffman, E.G. and **Sageman, B.B.** (1990) Biological sensing of benthic environments in dark shales and related oxygen-restricted facies. In: *Cretaceous Resources, Events and Rhythms*, pp. 121–138. Global Sedimentary Geology Program, Dordrecht, the Netherlands. https://doi.org/10.1007/978-94-015-6861-6_7.

Keller, G., **Berner, Z.**, **Adatte, T.** and **Stueben, D.** (2004) Cenomanian–Turonian and δ13C, and δ18O, sea level and salinity variations at Pueblo, Colorado. *Palaeogeogr. Palaeoclimatol. Palaeoecol.*, **211**, 19–43.

Knaust, D. (2017) *Atlas of Trace Fossils in Well Core: Appearance, Taxonomy and Interpretation*, p. 209. Springer, Alphen aan den Rijin.

Larson, R.L. and **Erba, E.** (1999) Onset of the mid-Cretaceous greenhouse in the Barremian-Aptian: igneous events and the biological, sedimentary, and geochemical responses. *Paleoceanography*, **14**, 663–678.

Laurin, J. and **Sageman, B.B.** (2007) Cenomanian Turonian coastal record in SW Utah, U.S.A.: Orbital-scale transgressive regressive events during Oceanic Anoxic Event II. *J. Sediment. Res.*, **77**(9), 731–756.

Lazar, O.R., **Bohacs, K.M.**, **Schieber, J.**, **Macquaker, J.H.S.** and **Demko, T.M.** (2015a) Mudstone primer: lithofacies variations, diagnostic criteria, and sedimentologic-stratigraphic implications at lamina to bedset scales. *SEPM Concepts Sedimentol. Paleontol.*, **12**, 198. https://doi.org/10.2110/sepmcsp.12.

Lazar, O.R., **Bohacs, K.M.**, **Macquaker, J.H.S.**, **Schieber, J.** and **Demko, T.M.** (2015b) Capturing key attributes of fine-grained sedimentary rocks in outcrops, cores, and thin sections: nomenclature and description guidelines. *J. Sed. Res.*, **85**, 230–246.

Leckie, R.M., **Yureitch, R.**, **West, O.**, **Finkelstein, D.** and **Schmidt, M.** (1998) Paleoceanography of the southwestern Western Interior Sea during the time of the Cenomanian-Turonian Boundary (Late Cretaceous). In: *Stratigraphy and Paleoenvironments of the Cretaceous Western Interior Seaway, U.S.A.* (Eds. Dean, W.E. and Arthur, M.A.), *SEPM Concepts in Sedimentology and Paleontology*, **6**, 101–126.

Leckie, R.M., **Bralower, T.J.** and **Cashman, R.** (2002) Oceanic anoxic events and plankton evolution: biotic response to tectonic forcing during the mid-Cretaceous. *Paleoceanography*, **17**, 3-1–13-29.

Leithold, E.L. (1993) Preservation of laminated shale in ancient clinoforms: comparison to modern subaqueous deltas. *Geology*, **21**, 359–362.

Leithold, E.L. and **Dean, W.E.** (1998) Depositional processes and carbon burial on a Turonian prodelta at the margin of the Western Interior Seaway. In: *Paleoenvironments of the Cretaceous Western Interior Seaway, USA* (Eds. MacEachern, J.A., Bann, K.L., Bhattacharya, J.B. and Howell, C.D.), *SEPM Concepts in Sedimentology and Paleontology*, **6**, 189–200.

Lockshin, S.N., **Yacobucci, M.M.**, **Gorsevski, P.** and **Gregory, A.** (2017) Spatial characterization of Cretaceous Western Interior Seaway paleoceanography using foraminifera, fuzzy sets and Dempster–Shafer theory. *GeoResJ*, **14**, 98–120.

Löwemark, L. and **Singh, A.** (2024) Influence of deep-reaching bioturbation on Arctic Ocean radiocarbon chronology. *Commun. Earth Environ.*, **5**, 293.

Lowery, C.M., **Corbett, M.J.**, **Leckie, R.M.**, **Watkins, D.**, **Miceli Romero, A.** and **Pramudito, A.** (2014) Foraminiferal and nannofossil paleoecology and paleoceanography of the Cenomanian-Turonian Eagle Ford Shale of southern Texas. *Palaeogeogr. Palaeoclimatol. Palaeoecol.*, **413**, 49–65.

Lowery, C.M., **Leckie, R.M.**, **Bryant, R.**, **Elderbak, K.**, **Parker, A.**, **Polyak, D.E.**, **Schmidt, M.**, **Snoeyenbos-West, O.** and **Sterzinar, E.** (2018) The Late Cretaceous Western Interior Seaway as a model for oxygenation change in epicontinental restricted basins. *Earth Sci. Rev.*, **177**, 545–564.

MacEachern, J.A. and **Bann, K.L.** (2020) The *Phycosiphon* ichnofacies and the *Rosselia* ichnofacies: two new ichnofacies for marine deltaic environments. *J. Sed. Res.*, **90**, 855–886.

MacEachern, J.A. and **Gingras, M.K.** (2007) Recognition of brackish-water trace fossil suites in the Cretaceous Western Interior Seaway of Alberta, Canada. In: *Sediment–Organism Interactions: A Multifaceted Ichnology* (Eds Bromley, R.G., Buatois, L.A., Mangano, M.G., Genise, J.F. and Melchor, R.N.), *SEPM Spec. Publ.*, **89**, 149–194.

MacEachern, J.A., **Bann, K.L.**, **Bhattachary, J.P.** and **Howell, C.D.** (2005) Ichnology of deltas: organism responses to the dynamic interplay of rivers, waves, storms, and tides. In: *River Deltas-Concepts*, *Models*, *and Examples* (Eds. L. Giosan and J.P. Bhattacharya), *SEPM*, **83**, 49–85.

MacEachern, J.A., **Pemberton, S.G.**, **Gingras, M.K.** and **Bann, K.L.** (2007) The ichnofacies paradigm: a fifty-year retrospective. In: *Trace Fossils* (Ed Miller, W.), pp. 52–77. Elsevier Amsterdam, Amsterdam, The Netherlands.

MacEachern, J.A., **Pemberton, G.**, **Bann, K.L.** and **Gingras, M.K.** (2012) Departures from the archetypal ichnofacies: effective recognition of physico-chemical stresses in the rock record. In: *Applied Ichnology* (Eds MacEachern, J.A., Bann, K.L., Gingras, M.K. and Pemberton, S.G.), *SEPM Short Course Notes*, **52**, 65–93.

Macquaker, J.H.S. (1987) The depositional and diagenetic history of the Westbury Formation (Upper Triassic) in south-west Britain. Doctoral Thesis, University of Bristol. Available at: https://research-information.bris.ac.uk/en/studentTheses/the-depositional-and-diagenetic-history-of-the-westbury-formation.

Macquaker, J.H.S. and **Adams, A.E.** (2003) Maximizing information from fine-grained sedimentary rocks: an inclusive nomenclature for mudstones. *J. Sed. Res.*, **73**, 735–744.

Macquaker, J.H.S., **Bentley, S.J.** and **Bohacs, K.M.** (2010) Wave-enhanced sediment-gravity flows and mud dispersal across continental shelves: Reappraising sediment transport processes operating in ancient mudstone successions. *Geology*, **38**, 947–950.

Martin, K.D. (2004) A re-evaluation of the relationship between trace fossils and dysoxia. *Geol. Soc. London Spec. Publ.*, **228**, 141–156.

Meyers, S.R. and **Sageman, B.B.** (2007) Quantification of deep-time orbital forcing by average spectral misfit. *Am. J. Sci.*, **307**, 773–792.

Meyers, S.R., **Sageman, B.B.** and **Hinnov, L.A.** (2001) Integrated quantitative stratigraphy of the Cenomanian Turonian Bridge Creek Limestone Member using evolutive harmonic analysis and stratigraphic modeling. *J. Sed. Res.*, **71**, 627–643.

Meyers, S.R., **Sageman, B.B.** and **Lyons, T.** (2005) Organic carbon burial rate and the molybdenum proxy: theoretical framework and application to Cenomanian-Turonian oceanic anoxic event 2. *Paleoceanography*, **20**, PA2002.

Monedero-Contreras, R.D., **Rodríguez-Tovar, F.J.** and **Martínez-Ruiz, F.** (2024) Impact of *Chondrites* on trace metal distribution in the sapropel S7 (ODP Site 966): implications for paleoenvironmental and paleoceanographic reconstructions. *Glob. Planet. Chang.*, **234**, 104387.

Monger, J.W.H., **Price, R.A.** and **Tempelman-Kluit, D.J.** (1982) Tectonic accretion and the origin of the two major metamorphic and plutonic welts in the Canadian Cordillera. *Geology*, **10**, 70–75.

Montoya-Pino, C., **Weyer, S.**, **Anbar, A.D.**, **Pross, J.**, **Oschmann, W.**, **van de Schootbrugge, B.** and **Arz, H.W.** (2010) Global enhancement of ocean anoxia during Oceanic Anoxic Event 2: a quantitative approach using U isotopes. *Geology*, **38**, 315–318.

Moore, P.G. and **Francis, C.H.** (1985) On the water relations and osmoregulation of the beach-hopper Orchestia Gammarellus (Pallas) (Crustacea: Amphipoda). *J. Mar. Biol. Ecol.*, **93**, 1131–1150.

O'Connor, L.K., **Jenkyns, H.C.**, **Robinson, S.A.**, **Remmelzwaal, S.R.**, **Batenburg, S.J.**, **Parkinson, I.J.** and **Gale, A.S.** (2020) A re-evaluation of the Plenus Cold Event, and the links between CO_2, temperature, and seawater chemistry during OAE 2. *Paleoceanogr. Paleoclimatol.*, **35**, e2019PA003631.

Ostrander, C.M., **Owens, J.D.** and **Nielsen, S.G.** (2017) Constraining the rate of oceanic deoxygenation leading up to a Cretaceous Oceanic Anoxic Event (OAE-2:~ 94 Ma). *Sci. Adv.*, **3**, e1701020.

Pană, D.I. and **van der Pluijm, B.A.** (2015) Orogenic pulses in the Alberta Rocky Mountains: radiometric dating of major faults and comparison with the regional tectono-stratigraphic record. *GSA Bull.*, **127**, 480–502.

Paz, M., **Mángano, M.G.**, **Buatois, L.A.**, **Desjardins, P.R.**, **Minisini, D.**, **Tomassini, F.G.**, **Rodríguez, M.N.**, **Pereira, E.** and **Parada, M.N.** (2023) An unusual oxygen-deficient ichnofauna from the Vaca Muerta Formation: implications for the ichnofacies model. *Lethaia*, **56**(4), 1–31.

Pemberton, S.G. and **Wightman, D.M.** (1992) Ichnological characteristics of brackish water deposits. In: *Applications of Ichnology to Petroleum Exploration*, *A Core Workshop* (Ed. Pemberton, S.G.), *SEPM Core Workshop*, **17**, 141–167.

Pemberton, S.G., **MacEachern, J.A.** and **Ranger, M.J.** (1992) Ichnology and event stratigraphy: the use of trace fossils in recognizing tempestites. In: *Applications of Ichnology to Petroleum Exploration*, *A Core Workshop* (Ed. Pemberton, S.G.), *SEPM Core Workshop*, **17**, 85–117.

Percival, L.M.E., **van Helmond, N.A.G.M.**, **Selby, D.**, **Goderis, S.** and **Claeys, P.** (2020) Complex interactions between large igneous province emplacement and global-temperature changes during the Cenomanian-Turonian Oceanic Anoxic Event (OAE 2). *Paleoceanogr. Paleoclimatol.*, **35**(10). https://doi.org/10.1029/2020pa004016.

Percy, E.L. (2021) Depositional processes and characterization of multi-scale heterogeneity of an organic-rich mudstone, Second White Specks Formation, SW Alberta. Doctoral Thesis, University of Calgary.

Percy, E.L. and **Pedersen, P.K.** (2020) Detailed facies analysis of Cenomanian–Turonian organic-rich mudstones: implications for depositional controls on source rocks. *Depositional Rec.*, **6**, 409–430.

Plint, A.G. (2014) Mud dispersal across a Cretaceous prodelta: storm-generated, wave-enhanced sediment gravity flows inferred from mudstone microtexture and microfacies. *Sedimentology*, **61**, 609–647.

Plint, A.G., **Macquaker, J.H.S.** and **Varban, B.L.** (2012) Bedload transport of mud across a wide, storm-influenced ramp: Cenomanian-Turonian Kaskapau Formation, Western Canada Foreland Basin. *J. Sed. Res.*, **82**, 801–822.

Polyak, D.E. (2003) Foraminiferal paleoceanography of the Cenomanian–Turonian Greenhorn cycle of the western side of the US Western Interior Sea. Master's thesis, University of Massachusetts.

Pratt, L.M. (1984) Influence of paleoenvironmental factors on preservation of organic matter in Middle Cretaceous Greenhorn Formation, Pueblo, Colorado. *AAPG Bull.*, **68**, 1146–1159.

Price, R.A. (1973) Large-scale gravitational flow of supracrustal rocks; southern Canadian Rockies. In: *Gravity and Tectonics* (Eds De Jong, K.A. and Scholton, R.A.), pp. 491–502. John Wiley and Sons, New York, NY.

Prokoph, A., **Babalola, L.O.**, **El Bilali, H.**, **Olagoke, S.** and **Rachold, V.** (2013) Cenomanian-Turonian carbon isotope stratigraphy of the Western Canadian Sedimentary Basin. *Cretac. Res.*, **44**, 39–53.

Quinn, G.M., **Hubbard, S.M.**, **Van Drecht, R.**, **Guest, B.**, **Matthews, W.A.** and **Hadlari, T.** (2016) Record of orogenic cyclicity in the Alberta Foreland basin, Canadian Cordillera. *Lithosphere*, **8**, 317–332.

Rees, E.I.S., **Nicholaidou, A.** and **Laskeridou, P.** (1977) The effects of storms on the dynamics of shallow water benthic associations. In: *Biology of Benthic Organisms* (Eds Keegan, B.F., Ceidigh, P.O. and Boaden, P.J.), pp. 465–474. Pergamon Press, Oxford, UK.

Rhoads, D.C. and **Morse, J.W.** (1971) Evolutionary and ecologic significance of oxygen-deficient marine basins. *Lethaia*, **4**, 413–428.

Ridgley, J.L., **Hester, T.C.**, **Condon, S.M.**, **Anna, L.O.**, **Rowan, E.L.**, **Cook, T.** and **Lillis, P.G.** (1999) Re-evaluation of the Shallow Biogenic Gas Accumulation, Northern Great Plains, USA – is similar gas accumulation in southeastern Alberta and southwestern Saskatchewan a good analog? *Sask. Geol. Surv. Summ. Investig.*, **1**, 1–78.

Rodríguez-Tovar, F.J. and **Dorador, J.** (2014) Ichnological analysis of Pleistocene sediments from the IODP Site U1385 "Shackleton Site" on the Iberian margin: approaching paleoenvironmental conditions. *Palaeogeogr. Palaeoclimatol. Palaeoecol.*, **409**, 24–32.

Rodríguez-Tovar, F.J., **Uchman, A.** and **Martín-Algarra, A.Í.** (2009) Oceanic anoxic event at the Cenomanian-Turonian boundary interval (OAE-2): ichnological approach from the Betic Cordillera, southern Spain. *Lethaia*, **42**, 407–417.

Sageman, B.B. (1989) The benthic boundary biofacies model: Hartland Shale Member, Greenhorn Formation (Cenomanian), Western Interior, North America. *Palaeogeogr. Palaeoclimatol. Palaeoecol.*, **74**, 87–110.

Sageman, B.B. and **Arthur, M.A.** (1994) Early Turonian paleogeographic/paleobathymetric map, Western Interior, US. In: *Mesozoic Systems of the Rocky Mountain Region, USA* (Eds. Caputo, M.V., Peterson, A. and Franczyk, K.J.), *Rocky Mountain Section*, *Society for Sedimentary Geology (SEPM)*, 457–469.

Sageman, B.B., **Meyers, S.R.** and **Arthur, M.A.** (2006) Orbital time scale and new C- isotope record for Cenomanian-Turonian boundary stratotype. *Geology*, **34**, 125–128.

Sageman, B.B., **Lyons, T.W.** and **Joo, Y.J.** (2013) Geochemistry of fine-grained, organic carbon-rich facies. In: *Treatise on Geochemistry (Second Edition)* (Eds Holland, H.D. and Turekian, K.K.), pp. 141–179. Elsevier, Oxford.

Sageman, B.B., **Jones, M.M.**, **Arthur, M.A.**, **Niezgodzki, I.** and **Horton, D.E.** (2024) Late Cenomanian Plenus event in the Western Interior Seaway. *Cretac. Res.*, **156**, 105798.

Sageman, B.B., **Rich, J.**, **Arthur, M.A.**, **Birchfield, G.E.** and **Dean, W.E.** (1997) Evidence for Milankovitch periodicities in Cenomanian-Turonian lithologic and geochemical cycles, Western Interior U.S.A. *SEPM J. Sediment. Res.*, **67**. https://doi.org/10.1306/d4268554-2b26-11d7-8648000102c1865d.

Savrda, C.E. (1995) Ichnologic applications in paleoceanographic, paleoclimatic, and sea-level studies. *Palaios*, **10**, 565.

Savrda, C.E. (1998) Ichnology of the Bridge Creek Limestone: evidence for temporal and spatial variations in paleo-oxygenation in the Western Interior Seaway. In: *Stratigraphy and Paleoenvironments of the Cretaceous Western Interior Seaway, USA* (Eds Dean, W.E. and Arthur, M.A.), *SEPM Concepts in Sedimentology and Paleontology*, **6**, 127–136.

Savrda, C.E. (2007) Trace fossils and marine benthic oxygenation. In: *Trace Fossils: Concepts, Problems, Prospects* (Ed Miller, W.I.), pp. 149–158. Elsevier, Amsterdam, The Netherlands.

Savrda, C.E. and **Bottjer, D.J.** (1986) Trace fossil model for reconstruction of paleo-oxygenation in bottom waters. *Geology*, **14**, 3–6.

Savrda, C.E. and **Bottjer, D.J.** (1987) Trace fossils as indicators of bottom-water redox conditions in ancient marine environments. In: *New Concepts in the Use of Biogenic Sedimentary Structures for Paleoenvironmental Interpretation* (Ed. D.J. Bottjer), *SEPM*, **52**, 3–26.

Savrda, C.E. and **Bottjer, D.J.** (1989) Anatomy and implications of bioturbated beds in "black shale" sequences: examples from the Jurassic Posidonienschiefer (Southern Germany). *Palaios*, **4**, 330.

Savrda, C.E. and **Bottjer, D.J.** (1991) Oxygen-related biofacies in marine strata: an overview and update. *Geol. Soc. London Spec. Publ.*, **58**, 201–219.

Savrda, C.E. and **Bottjer, D.J.** (1994) Ichnofossils and ichnofabrics in rhythmically bedded pelagic/hemi-pelagic carbonates: recognition and evaluation of benthic redox and scour cycles. In: *Orbital Forcing and Cyclic Sequences* (Eds de Boer, P.L. and Smith, D.G.), *IAS Spec. Publ.*, 19, 195–210.

Schieber, J. (1994) Evidence for high-energy events and shallow-water deposition in the Chattanooga Shale, Devonian, central Tennessee, USA. *Sed. Geol.*, **93**, 193–208.

Schieber, J. (1998) Sedimentary features indicating erosion, condensation, and hiatuses in the Chattanooga Shale of Central Tennessee: relevance for sedimentary and stratigraphic evolution. In: *Shales and Mudstones: Basin Studies, Sedimentology and Paleontology* (Eds Schieber, J., Zimmerle, W. and Sethi, P.S.), pp. 187–215. Schweizerbart, Stuttgart.

Schieber, J. (2003) Simple gifts and buried treasures—implications of finding bioturbation and erosion surfaces in black shales. *Sed. Rec.*, **1**, 4–8.

Schieber, J. and **Wilson, R.D.** (2021) Burrows without a trace—how meioturbation affects rock fabrics and leaves a record of meiobenthos activity in shales and mudstones. *PalZ*, **95**, 767–791.

Schieber, J., **Shao, X.**, **Yawar, Z.** and **Liu, B.** (2021) Cryptic burrow traces in black shales – a petrographic Rorschach test or the real thing? *Sedimentology*, **68**, 2707–2731.

Schlanger, S.O. and **Jenkyns, H.C.** (1976) Cretaceous oceanic anoxic events: causes and consequences. *Geol. Mijnb.*, **55**, 179–184.

Schlanger, S.O., **Arthur, M.A.**, **Jenkyns, H.C.** and **Scholle, P.A.** (1987) The Cenomanian-Turonian Oceanic Anoxic Event, I. stratigraphy and distribution of organic carbon-rich beds and the marine δ13C excursion. *Geol. Soc. London Spec. Publ.*, **26**, 371–399.

Schröder-Adams, C.J., **Leckie, D.A.**, **Bloch, J.**, **Craig, J.**, **McIntyre, D.J.** and **Adams, P.J.** (1996) Paleoenvironmental changes in the Cretaceous (Albian to Turonian) Colorado group of western Canada: microfossil, sedimentological and geochemical evidence. *Cretac. Res.*, **17**, 311–365.

Scott, C. and **Lyons, T.W.** (2012) Contrasting molybdenum cycling and isotopic properties in euxinic versus non-euxinic sediments and sedimentary rocks: refining the paleoproxies. *Chem. Geol.*, **324–325**, 19–27.

Seilacher, A. (1982) Distinctive features of sandy tempestites. In: *Cyclic and Event Stratification* (Eds Einsele, G. and Seilacher, A.), pp. 333–349. Springer, Berlin, Heidelberg, Berlin.

Singer, B.S., **Jicha, B.R.**, **Sawyer, D.A.**, **Walaszczyk, I.**, **Landman, N.**, **Sageman, B.B.** and **McKinney, K.C.** (2025) A 40Ar/39Ar and U–Pb timescale for the Cretaceous Western Interior Basin, North America. *Geol. Soc. London Spec. Publ.*, **544**, SP544-2023.

Slingerland, R., **Kump, L.R.**, **Arthur, M.A.**, **Fawcett, P.J.**, **Sageman, B.B.** and **Barron, E.J.** (1996) Estuarine circulation in the Turonian Western Interior Seaway of North America. *GSA Bull.*, **108**, 941–952.

Smith, C.R., **Levin, L.A.**, **Hoover, D.J.**, **McMurtry, G.** and **Gage, J.D.** (2000) Variations in bioturbation across the oxygen minimum zone in the northwest Arabian Sea. *Deep Sea Res. Part II Top. Stud. Oceanogr.*, **47**, 227–257.

Sperling, E.A., **Frieder, C.A.**, **Raman, A.V.**, **Girguis, P.R.**, **Levin, L.A.** and **Knoll, A.H.** (2013) Oxygen, ecology, and the Cambrian radiation of animals. *Proc. Natl Acad. Sci. USA*, **110**, 13446–13451.

Stasiuk, L.D. and **Goodarzi, F.** (1988) Organic petrology of Second White Speckled Shale, Saskatchewan, Canada – a possible link between bituminite and biogenic gas? *Bull. Can. Petrol. Geol.*, **36**, 397–406.

Stel, J.H. (1975) The influence of hurricanes upon the quiet depositional conditions in the Lower Emsian Lavid Shales of Colle (NW Spain). *Leidse. Geol. Meded.*, **49**, 475–486.

Synnott, D.P., **Dewing, K.**, **Sanei, H.**, **Pedersen, P.K.** and **Ardakani, O.H.** (2017) Influence of refractory organic matter on source rock hydrocarbon potential: a case study from the Second White Specks and Belle Fourche formations, Alberta, Canada. *Mar. Pet. Geol.*, **85**, 220–232.

Takashima, R., **Nishi, H.**, **Huber, B.** and **Leckie, R.M.** (2006) Greenhouse world and the Mesozoic Ocean. *Oceanography*, **19**, 82–92.

Taylor, A.M. and **Goldring, R.** (1993) Description and analysis of bioturbation and ichnofabric. *J. Geol. Soc. Lond.*, **150**, 141–148.

Timmer, E.R., **Botterill, S.E.**, **Gingras, M.K.** and **Zonneveld, J.-P.** (2016) Visualizing a process ichnology dataset, Lower Cretaceous McMurray Formation, NE Alberta, Canada. *Bull. Can. Petrol. Geol.*, **64**, 251–265.

Trabucho Alexandre, J., **Tuenter, E.**, **Henstra, G.A.**, **van der Zwan, K.J.**, **van de Wal, R.S.W.**, **Dijkstra, H.A.** and **de Boer, P.L.** (2010) The mid-Cretaceous North Atlantic nutrient trap: black shales and OAEs. *Paleoceanography*, **25**, PA4201.

Turgeon, S.C. and **Creaser, R.A.** (2008) Cretaceous oceanic anoxic event 2 triggered by a massive magmatic episode. *Nature*, **454**, 323–326.

Tyagi, A., **Plint, A.G.** and **McNeil, D.H.** (2007) Correlation of physical surfaces, bentonites, and biozones in the Cretaceous Colorado Group from the Alberta Foothills to southwest Saskatchewan, and a revision of the Belle Fourche – Second White Specks formational boundary. *Can. J. Earth Sci.*, **44**, 871–888.

Tyson, R.V. (1987) The genesis and palynofacies characteristics of marine petroleum source rocks. In: *Marine Petroleum Source Rocks* (Eds Brooks, J. and Fleet, A.J.), *Geol. Soc. Lond. Spec. Publ.*, **26**, 47–67.

Tyson, R.V. and **Pearson, T.H.** (1991) Modern and ancient continental shelf anoxia: an overview. *Geol. Soc. London Spec. Publ.*, **58**, 1–24.

Tyszka, J. (1994) Paleoenvironmental implications from ichnological and microfaunal analyses of Bajocian spotty carbonates, Pieniny Klippen Belt, Polish Carpathians. *Palaios*, **9**, 175–187.

Vermeij, G.J. (1995) Economics, volcanoes, and Phanerozoic revolutions. *Paleobiology*, **21**, 125–152.

Walker-Trivett, C.A., **Kender, S.**, **Bogus, K.A.**, **Littler, K.**, **Edvardsen, T.**, **Leng, M.J.**, **Lacey, J.**, **Riding, J.B.**, **Miller, I.L.** and **Wagner, D.** (2024) Oceanic Anoxic Event 2 triggered by Kerguelen volcanism. *Nat. Commun.*, **15**, 5124.

Wan, X., **Wignall, P.B.** and **Zhao, W.** (2003) The Cenomanian-Turonian extinction and oceanic anoxic event: evidence from southern Tibet. *Palaeogeogr. Palaeoclimatol. Palaeoecol.*, **199**, 283–298.

Wells, G.C. (1957) The Sweetgrass Arch area – Southern Alberta. Canadian Society of Petroleum Geologists, Guide Book Seventh Annual Field Conference Waterton.

Westermann, S., **Caron, M.**, **Fiet, N.**, **Fleitmann, D.**, **Matera, V.**, **Adatte, T.** and **Föllmi, K.B.** (2010) Evidence for oxic conditions during oceanic anoxic event 2 in the northern Tethyan pelagic realm. *Cretac. Res.*, **31**, 500–514.

Wetzel, A. (1983) Biogenic sedimentary structures in a modern upwelling region: northwest African continental margin. In: *Costal Upwelling and its Sediment Record, Part B, Sedimentary Records of Ancient Costal Upwelling* (Eds Thiede, J. and Suess, E.), pp. 123–144. Plenus, New York, NY.

Wetzel, A. (1991) Ecologic interpretation of deep-sea trace fossil communities. *Palaeogeogr. Palaeoclimatol. Palaeoecol.*, **85**, 47–69.

Wetzel, A. and **Bromley, R.G.** (1994) *Phycosiphon incertum* revisited: *Anconichnus horizontalis* is its junior subjective synonym. *J. Paleontol.*, **68**, 1396–1402.

Wetzel, A. and **Uchman, A.** (1998) Biogenic sedimentary structures in mudstones: an overview. In: *Shales and Mudstones*, *Volume I* (Eds Schieber, J., Zimmerle, W. and Sethi, P.), *Basin Studies*, *Sedimentology*, *and Paleontology*, pp. 351–369.

Wetzel, A. and **Uchman, A.** (2001) Sequential colonization of muddy turbidites in the Eocene Beloveza Formation, Carpathians, Poland. *Palaeogeogr. Palaeoclimatol. Palaeoecol.*, **168**, 171–186.

Wignall, P.B. (1991) Dysaerobic trace fossils and ichnofabrics in the Upper Jurassic Kimmeridge Clay of Southern England. *Palaios*, **6**, 264–270.

Wignall, P.B. and **Myers, K.J.** (1988) Interpreting benthic oxygen levels in mudrocks: a new approach. *Geology*, **16**, 452–455.

Wilmsen, M., **Niebuhr, B.**, **Wood, C.J.** and **Zawischa, D.** (2007) Fauna and palaeoecology of the Middle Cenomanian Praeactinocamax primus Event at the type locality, Wunstorf quarry, northern Germany. *Cretac. Res.*, **28**(3), 428–460.

Wright, G.N. (1994) Structure and Architecture of the Western Canada Sedimentary Basin. In: *Geologic Atlas of* *the Western Canadian Sedimentary Basin* (Eds Mossop, G.D. and Shetsen, I.), Canadian Society of Petroleum Geologists and Alberta Research Council. Available at: https://ags.aer.ca/atlas-the-western-canada-sedimentary-basin/chapter-28-geological-history-the-peace-river-arch, [January 20th, 2025].

Manuscript received 25 October 2024; revision accepted 10 November 2025

Supporting Information

Additional information may be found in the online version of this article:

Data S1. Detailed description and occurrence of ichnogenera and other biodeformational features.